INTERNATIONAL ATOMIC ENERGY AGENCY
UNITED NATIONS EDUCATIONAL, SCIENTIFIC AND CULTURAL ORGANIZATION
INTERNATIONAL CENTRE FOR THEORETICAL PHYSICS
I.C.T.P., P.O. BOX 586, 34100 TRIESTE, ITALY, CABLE CENTRATOM TRIESTE

SMR.764 - 6

RESEARCH WORKSHOP ON CONDENSED MATTER PHYSICS
13 JUNE - 19 AUGUST 1994

WORKING GROUP ON
"DISORDERED ALLOYS"
8 - 19 AUGUST 1994

"Buckled structures of mixed crystals"

Alexander VORONEL
Tel-Aviv University
Raymond & Beverly Sackler Faculty of Exact Sciences
School of Physics & Astronomy
ISRAEL

These are preliminary lecture notes, intended only for distribution to participants

Buckled Crystalline Structure of Mixed Ionic Salts

A. Frenkel,[1] E. A. Stern,[2] A. Voronel,[1] M. Qian,[2] and M. Newville[2]
[1]*School of Physics and Astronomy, Tel Aviv University, Ramat Aviv 69978, Israel*
[2]*Department of Physics, FM-15, University of Washington, Seattle, Washington 98195*
(Received 21 July 1993)

X-ray absorption fine structure (XAFS) measurements of mixed salts $Rb_xK_{1-x}Br$ and $RbBr_yCl_{1-y}$ at their congruent melting points compositions reveal that their actual structure buckles about the NaCl average structure with an rms angular deviation from collinearity of 7°–9°. XAFS measures the buckling directly through three-body correlations, and verifies the homogeneity and randomness of the mixtures. The characteristic ionic sizes are found to be dependent on concentration, causing changes to 0.1 Å in interatom bond distances. A computer simulation based on the information from XAFS and diffraction displays the actual structure of the salts.

PACS numbers: 61.10.Lx, 61.60.+m, 78.70.Dm

It is generally agreed that a fundamental understanding of the properties of a solid starts with the knowledge of its atomic structure. For pure compounds and elements, generally, especially at low temperature, the position of every atom is on a periodic array. The recently discovered aperiodic crystals are exceptions to this rule but it is believed that the ideal crystals of this type also have perfect long-range order.

When the solid is composed of an alloy or mixture of atoms or molecules over a range of compositions and still remains a single phase, the perfect periodicity is broken by the randomness of the mixing and the difference in the type of atoms. Yet, the average structure still remains periodic and produces sharp Bragg diffraction peaks. However, the actual distribution of atoms usually will not be centered on the periodic lattice. The problem could be further complicated by short range order such as a positive or negative tendency of like atoms to cluster. The issue of the actual location of atoms in such cases relative to the average lattice has not yet, to our knowledge, been addressed experimentally.

In this Letter we investigate this issue for the mixed ionic salts $Rb_xK_{1-x}Br$ and $RbBr_yCl_{1-y}$, where the cations sublattice is disordered in the former and the anion in the latter. The x-ray absorption fine structure (XAFS) technique is used in our investigation because it enables us to obtain both partial pair and three-body correlation functions, which as we show, give sufficient information to completely specify the actual structure.

The two mixtures of interest are soluble in the solid for all compositions. The composition of the mixed salts that were investigated was chosen at the congruent melting point, namely, the minimum of the melting temperature where the liquidus and solidus lines are tangent at their intersection and the solid and liquid have the same equilibrium composition (Fig. 1). This occurs at $x = 0.76$ for $Rb_xK_{1-x}Br$ and $y = 0.62$ for $RbBr_yCl_{1-y}$ [1,2]. For such a composition the solidification occurs at a single temperature, producing a homogeneous single phase solid. The resultant solid was ground and sieved through 400 mesh. The powder was placed in a quartz tube and heated to 120 °C for several hours while being evacuated by a mechanical pump in order to drive off any absorbed water, and then sealed under vacuum. The container was opened in a dry nitrogen atmosphere, rubbed onto Scotch tape, and then the appropriate number of layers were stacked and sealed in a vacuum tight sample cell under the dry nitrogen atmosphere. The procedure ensured the sample did not contain a significant amount of water.

XAFS measurements were performed at the National Synchrotron Light Source (NSLS) on beamline X11A using a double crystal Si(111) monochromator. Care was taken to eliminate sources of distortion of the XAFS signal (such as minimizing harmonics by detuning the monochromator and making the absorption per layer of sample much less than an absorption length). Measure-

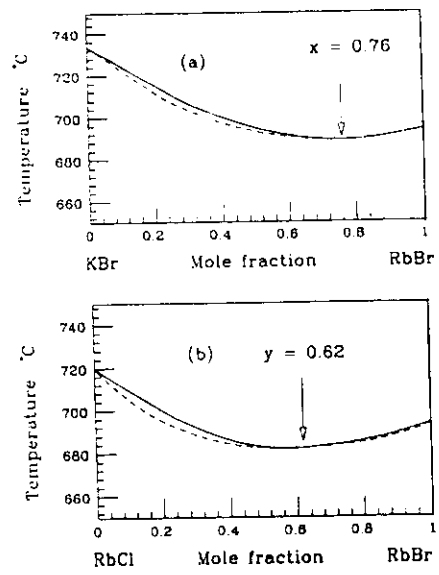

FIG. 1. Phase diagrams of binary mixtures: (a) KBr and RbBr, and (b) RbCl and RbBr. Solid line: liquidus; dashed line: solidus. Arrows indicate the congruent melting minima concentrations.

0031-9007/93/71(21)/3485(4)$06.00

ments were performed on samples whose temperatures were controlled by a Displex refrigerator. Helium gas within the sample cell (windows of 2 mil Kapton) assured good thermal contact between the Cu cell and the powder samples below liquid nitrogen temperatures.

The XAFS spectra were taken at the Rb and Br K edges of the two mixed salt samples at 30 K. The background was subtracted using the program AUTOBK [3]. A typical resultant normalized XAFS signal $k\chi(k)$ is shown in Fig. 2, where k is the wave number of the photoelectron referenced to the Fermi energy. Both AUTOBK and subsequent fits of the $\chi(k)$ used theoretical calculations of FEFF5 [4]. The theory contains empirical parameters which were determined from the constituent pure salts [5] by enforcing agreement with their known structure.

FEFF5 calculates the contribution to the XAFS of single scattering (SS) and multiple scattering (MS) paths of the photoelectron as it scatters from the surrounding atoms. Since the structure of the mixed salts is, on the average, of NaCl form, and, as we will show, the deviations from this average are small, we could be guided by the analysis of the pure salts to predict which MS paths were negligible, particularly those that have a 90° angle between the outgoing and incoming paths [6]. The end result was that the XAFS signal is dominated by SS paths and those MS paths which are formed by three collinear (or nearly so) atoms. The good agreement that FEFF5 obtains with the pure salts [5], which requires, among others, accurate calculation of the collinear MS paths, gives us confidence that it can also calculate accurately these MS paths when they deviate slightly from collinearity, as in the mixed salts.

The fitting of a theoretical XAFS $\chi(k)$ to the experimental signal was done in r space. The fitting algorithm of the computer code FEFFIT [7] is based on a standard nonlinear least squares technique which minimizes the difference between the Fourier transformed theoretical and experimental χ's. As variables FEFFIT uses the structural characteristics of the sample data: R_i, interatomic distances, σ_i^2, mean square deviations in the half path lengths (XAFS Debye-Waller factor), and ΔE_i shifts to the E_0 overall, the photoelectron energy origin. An additional parameter S_0^2 (the passive electrons reduction factor for the central atom [8]) was fixed to be the same as that found for the pure salts [5] for each of the two central atoms, namely, 0.91 for Br and 0.98 for Rb.

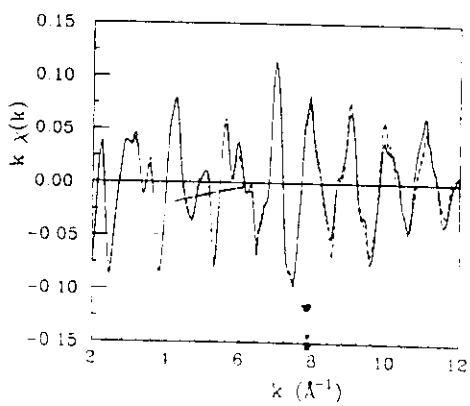

FIG. 2. Normalized absorption $k\chi(k)$ of two independent measurements (dashed and solid) of the Br edge of $Rb_{0.76}K_{0.24}Br$.

The accuracy of the analysis was tested by fitting the first neighboring (1nn) shell about the atom of the ordered sublattice, the common Br (Rb) atom. In that case the concentration of the 1nn two anions (cations) must agree with the average composition of the mixture regardless of any tendency to cluster. Indeed an agreement was found for the two salt mixtures within the uncertainty of 1%. Next, the fit was made to the second neighbor (2nn) shell about the Rb (Br) in the disordered sublattice. The composition of the 2nn would differ from x (y) if there were any tendency for clustering. The 2nn is on the same disordered sublattice as the center atom and ascertains the concentration of the two types of atoms that reside on this sublattice. In both mixtures, the compositions determined with 2nn agreed again with x or y within the uncertainty of 1%, indicating that the cations or anions, respectively, are completely randomly distributed in their sublattices, and thus there is no short range ordering.

Up to now the analysis was dominated by only SS. The next interesting shell to be analyzed is the fourth nearest neighbor (4nn) about an atom on the ordered sublattice. In the NaCl structure the 4nn, 1nn, and the center atom are collinear. Such a collinear alignment increases significantly the contribution of the 4nn to the XAFS signal by the forward multiple scatterings through the 1nn intervening atom [9]. This so-called focusing effect turns out to be a very sensitive function of the angular deviation from collinearity and can therefore be used to obtain an accurate measure of it [10,11], as long as it is small enough (less than 20°). By choosing the center atom on the ordered sublattice the 1nn intervening atom is on the disordered sublattice, and thus is of two kind, while the 4nn is the same kind as the center atom. Table I gives the result of such an analysis of the angular deviation from collinearity, $\langle\Theta^2\rangle^{1/2}$. The final fit in r space of $Rb_{0.76}K_{0.24}Br$ (Br edge) to the data is shown in Fig. 3, illustrating the good agreement over the fitting range up to 8 Å.

Also given in Table I are the 4nn, 1nn, and the averaged 1nn distances from the common atom in the two mixtures. The averaging is done over the composition. If the structure had these atoms in a collinear configuration, the 4nn distance would be twice the averaged 1nn distance. Twice the averaged 1nn distance is 0.03 Å larger than the 4nn distance for both samples, consistent with the buckling of the lattice about collinearity. Note that this evidence for buckling is independent of the direct measure of $\langle\Theta^2\rangle$ obtained from the focusing effect.

The other point to note from Table I is the difference of the 1nn distance in the mixed salts from the corre-

TABLE I. Nearest bond lengths r_{1nn} (in Å) and Debye-Waller factors σ^2_{1nn} (in 10^{-3} Å^2) in RbBr, KBr, RbCl (superscript "pure") and their mixtures $Rb_{0.76}K_{0.24}Br$ and $RbBr_{0.62}Cl_{0.38}$ (superscript "mix"). The column $\langle r^{mix}_{1nn}\rangle$ gives the 1nn bond distances averaged over composition. r^{mix}_{4nn} is the fourth neighbor distance (in Å) and the last column gives the buckling angles in degrees.

	Bond	r^{mix}_{1nn}	$\langle r^{mix}_{1nn}\rangle$	r^{pure}_{1nn}	$\sigma^{2(mix)}_{1nn}$	$\sigma^{2(pure)}_{1nn}$	r^{mix}_{4nn}	rms $\langle\Theta\rangle$
$Rb_{0.76}K_{0.24}Br$	Br-Rb	3.39(1)	3.385(10)	3.41(1)	6.0(5)	5.5(5)	6.74(1)	Br-Rb-Br:9.0(1.6)
	Br-K	3.37(1)	3.385(10)	3.27(1)	6.4(5)	6.1(5)	6.74(1)	Br-K-Br:7.7(2.7)
$RbBr_{0.62}Cl_{0.38}$	Rb-Br	3.39(1)	3.371(10)	3.41(1)	6.0(5)	5.5(5)	6.71(1)	Rb-Br-Rb:8.2(1.5)
	Rb-Cl	3.34(1)	3.371(10)	3.27(1)	9.6(5)	5.5(5)	6.71(1)	Rb-Cl-Rb:7.3(3.0)

sponding values of the pure salts and their respective σ^2, mean squared disorder about the distance. For instance, the Br-K 1nn distance changes from 3.27 Å in the pure salt to 3.37 Å in the mixed salt with no significant increase in σ^2. This large change of 0.1 Å with no change in σ^2 indicates that the size of these ions is concentration dependent. Just the fact the bond distance changes is not, by itself, sufficient evidence of a change in size of the ions because, as pointed out by Ashcroft and Mermin [12], the ions may not be "touching." The evidence of touching, though, is reflected by the σ^2 since this is a measure, at the low temperatures of the measurements, of the zero point motion and thus the contact force between atoms. The lack of change in σ^2 indicates the same contact force, and thus "touching" for both distances of this mixture. In contrast, the Rb-Cl 1nn distance increases in the mixed salt over the pure salt by 0.07 Å. Yet the σ^2 also almost doubles (see Table I), suggesting that the contact present in the pure salt is loosened in the mixture and the increase in bond length should not be interpreted as an increase in ionic size. Boyce and Mikkelsen [13] also pointed out that the alkali halide 1nn bonds are functions of concentration but their conclusion that the size of the atoms correspondingly changed was not validated since no check was made on the corresponding changes in σ^2. One expects that the negatively charged Br ion can be distorted more easily than the positively charged K core and thus it is likely that the negative ion has the more variable size.

The XAFS determined the average and mean squared variation, σ^2, of the atomic distances from the center

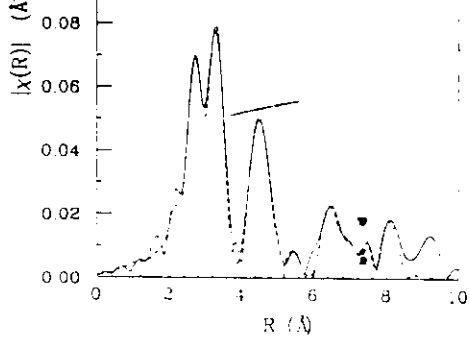

FIG. 3. Fit of the magnitude of the theoretical $\chi(R)$ (dashed line) to $Rb_{0.76}K_{0.24}Br$, Br edge data (solid line).

atom. It also determined the mean squared angular deviation from collinearity (*buckling* angle), $\langle\Theta^2\rangle$, and the random distribution of the atoms on the disordered sublattice. This information, together with the knowledge of the average structure as determined by diffraction, is sufficient to obtain the *actual* distribution of atoms in the mixture by a molecular dynamics simulation. Since the anharmonicity of the atomic vibrations was found to be negligible at 30 K where the data were taken and analyzed, harmonic potentials between pairs of nearest neighbors were assumed and set to give those values of σ^2 determined for the pure salts [5]. The minima of the potentials were set at the average relative positions determined by XAFS. Our results were not sensitive to assumption of the harmonic potentials, only to the relative positions of the minima.

The structure of the mixed salts was calculated by the molecular-dynamics computer code CLUSTER [14] which gave good agreement with experiment for the simulation of the pure constituent alkali halides [14]. The calculations were performed over both $9 \times 9 \times 9$ (729 atoms), and $11 \times 11 \times 11$ (1331 atoms) clusters in order to check for surface effects. The arbitrary initial configuration of the AB_xC_{1-x} salt was prepared using a random numbers generator for placing the B and C atoms on their average sublattice sites in accordance with the concentration. Atoms A were also placed on their average sublattice. During the simulation, the surface atoms were kept fixed while the internal atoms were allowed to move in accordance with the classical equations of motion and initial random velocities which were rescaled downward several times until the atoms attained a stable equilibrium configuration in the potential minimum. A time step of 10^{-15} s was chosen, which is more than an order of magnitude smaller than the vibrational period. For both clusters averaging was done over the inner $5 \times 5 \times 5$ cluster to exclude the influence of the fixed surface atoms. For the larger cluster, averaging was also done over the inner $7 \times 7 \times 7$ cluster to verify that the averaged region had been immersed into the interior deeply enough to be insulated from surface effects. The final values were obtained by time averaging over 2×10^{-11} s during the last run of the program where the desired equilibrium was achieved. The results obtained in all cases agreed with one another to about 0.1°, indicating that surface effects were negligible.

The simulation results were in good agreement

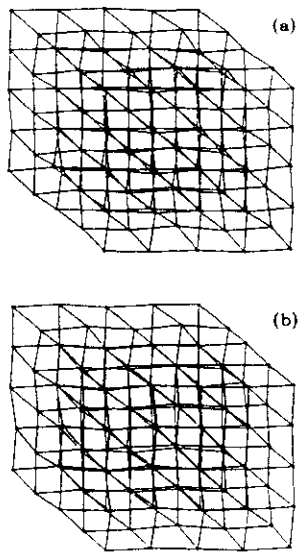

FIG. 4. Equilibrium cluster (inner 125 atoms) configurations of $Rb_{0.76}K_{0.24}Br$ (a) and $RbBr_{0.62}Cl_{0.38}$ (b).

with our XAFS results, e.g., the rms buckling angles were Θ(Br-Rb-Br) = 8.2°, Θ(Br-K-Br) = 8.0° in $Rb_{0.76}K_{0.24}Br$ and Θ(Rb-Br-Rb) = 8.8°, Θ(Rb-Cl-Rb) = 8.0° in $RbBr_{0.62}Cl_{0.38}$, agreeing within uncertainties with the measurements and the uncertainties of the parameters of the model. The resultant structures obtained by the simulation display the actual equilibrium positions of the atoms. Figures 4(a) and 4(b) show the buckled structure within the $Rb_{0.76}K_{0.24}Br$ and $RbBr_{0.62}Cl_{0.38}$ (inner 125 atoms) clusters, respectively.

The fundamental understanding of alloys (and mixed salts) is presently in a rather primitive state. At one empirical level the relative size of the atoms is a parameter that has been correlated with the solubility limits of one with the other. When the size difference exceeds a critical value complete solubility does not occur for all concentrations [15]. At another empirical level, electron per atom ratios are correlated with solubilty limits [16]. On a fundamental level, theoretical approximations have been developed to calculate the electronic properties of alloys, but these models neglect the local deviations from the average structure [17].

It is clear that these distortions are important for understanding the properties of alloys, e.g., the dependence of melting temperature and solubility limits on atomic size differences [18]. Our measurements, however, show that the concept of a rigid atomic size does not apply to the alkali halides, indicating that their understanding requires more sophisticated considerations.

Our XAFS measurements have also shown directly that the actual structure of the mixed salts buckles about the average NaCl structure. This result is possible because XAFS is capable of directly measuring *three* body correlations with high accuracy when the three atoms are near collinearity. The angle of this buckling is a new parameter which should be added to the characteristics of the structure needed to fully understand the properties of the mixed crystals. It is reasonable to expect that this buckling is a general phenomenon of all disordered lattices.

In conclusion, it is not necessary to be limited in calculating the properties of alloys or mixed salts by simply placing atoms at their average positions. XAFS adds additional information allowing the determination of the actual positions of the atoms in the mixed systems, opening up the prospect of more accurate calculations of the properties of such materials.

This work was supported in part by DOE Grant No. DE-FG06-90ER45425 and by the U.S.-Israel BNSF Grant No. 90-00152/1. Two of us (A.F. and A.V.) acknowledge the hospitality of the XAFS laboratory at the University of Washington where this work was carried out and we all wish to thank B. Ravel, S. Zabinsky, and Professor J. J. Rehr for stimulating discussions.

[1] J. Sangster and A. D. Pelton, J. Phys. Chem. Ref. Data **16**, 509 (1987).
[2] D. Berrebi, L. Grigoryan, S. Rabinovich, E. Shasha, and A. Voronel, J. Phys. Condens. Matter **4**, 10139 (1992).
[3] M. Newville, P. Livins, Y. Yacoby, J. J. Rehr, and E. A. Stern, Phys. Rev. B **47**, 14126 (1993).
[4] J. J. Rehr, R. C. Albers, and S. I. Zabinsky, Phys. Rev. Lett. **69**, 3397 (1992); J. Mustre de Leon, J. J. Rehr, S. I. Zabinsky, and R. C. Albers, Phys. Rev. B **44**, 4146 (1991).
[5] A. I. Frenkel, E. A. Stern, M. Qian, and M. Newville, Phys. Rev. B. **48**, 12449 (1993).
[6] G. Bunker and E. A. Stern, Phys. Rev. Lett. **52**, 1990 (1985).
[7] M. Newville (unpublished).
[8] E. A. Stern and S. M. Heald, in *Handbook on Synchrotron Radiation*, edited by E. E. Koch (North-Holland, New York, 1983), Vol. 1.
[9] P. A. Lee and J. B. Pendry, Phys. Rev. B **11**, 2795 (1975).
[10] B.-K. Teo, J. Am. Chem. Soc. **103**, 3990 (1981).
[11] B. Rechav, N. Sicron, Y. Yacoby, B. Ravel, M. Newville, and E. A. Stern, Physica (Amsterdam) **209C**, 55 (1993).
[12] N. W. Ashcroft and N. D. Mermin, *Solid State Physics* (Saunders, Philadelphia, 1976), pp. 382–385.
[13] J. Boyce and J. C. Mikkelsen, Jr., Phys. Rev. B **31**, 6903 (1985).
[14] A. Frenkel, E. Shasha, O. Gorodetsky, and A. Voronel, Phys. Rev. B **48**, 1283 (1993).
[15] A. Voronel, S. Rabinovich, A. Kisliuk, V. Steinberg, and T. Sverbilova, Phys. Rev. Lett. **60**, 2402 (1988).
[16] W. Hume-Rothery, J. Inst. Met. **35**, 295 (1926); **35**, 307 (1926).
[17] See, e.g., *Excitations in Disordered Systems*, edited by F. Thorpe (Plenum, New York, 1981).
[18] S. Rabinovich, A. Voronel, and L. Peretzman, J. Phys. C **21**, 5943 (1988).

Comparative radial-distribution analysis of the short range order in metallic glass $Al_{0.91}La_{0.09}$ and crystalline $Al_{11}La_3$

A. Frenkel[a], A. Rubshtein[a], A. Voronel[a] and E. A. Stern[b]

[a] R. & B. Sackler Sch. of Phys. and Astr. , Tel Aviv Univ., Tel Aviv 69978, Israel
[b] Department of Physics FM-15, University of Washington, Seattle, WA 98195, USA

XAFS data of metallic glass $Al_{0.91}La_{0.09}$ and a crystalline phase $Al_{11}La_3$ formed by annealing of the glass were measured at the La L_3 edge at T=12 K and analyzed using the radial distribution function method. The shortest La-Al distance appeared to be distinctively smaller within the glass than in the crystal. This difference decreases the disparity in size of La and Al in the alloy, allowing their mixing in the glassy state.

The metallic glass $Al_{0.91}La_{0.09}$ was recently synthesized by a melt-spinning method [1]. The purpose of the present work was to examine the structure of this alloy by XAFS for better understanding of the reason for the unusual glass formation at high concentration of Al (> 90 %). We found that a small fraction of La - Al bonds in the glass shortened by 0.12 ± 0.05 Å as a result of the quenching process. This decreases the size disparity of La and Al atoms, allowing their mixing into the single glassy phase.

We used both an X-ray diffraction method to characterize the samples and the RDF method of XAFS [2] to study the local atomic environment around the central La atoms. We tested the RDF method first against the known structure ($Al_{11}La_3$) to check the reliability of the method.

Amorphous ribbons of metallic glass $Al_{0.91}La_{0.09}$ were produced by melt spinning in the Technion (Israel) and rolled to 20 μm thickness to avoid the thickness effect in XAFS by satisfying the condition $\Delta\mu x \leq 1$, x being the sample thickness and $\Delta\mu$ the absorption L_3 edge step. The crystalline phase $Al_{11}La_3$ was obtained by annealing some of the ribbons. X-ray diffraction measurements showed large crystallites of Al and $Al_{11}La_3$ phases in the crystallized ribbons. The XAFS measurements on the La L_3 edge (photon energy is 5483 eV) were performed on the beamline X11A at NSLS using a double crystal (111) Si monochromator. The data were obtained at 12 K. The AUTOBK code [3] was used to extract the atomic background for both glass and crystal data. The resultant $\chi(k)$, where k is the photoelectron wavenumber, was normalized to the L_3- edge jump. Special care was taken to determine correctly the $k = 0$ point. Since the photoelectron transition occurs to the first unoccupied level, the lowest possible wavenumber is the Fermi momentum k_f. To achieve the true $k = 0$ limit we determined the Fermi energy level while using FEFF5 theory [4] to subtract background [3] and then lowered the energy reference by E_f. The values of k_f and E_f are provided by FEFF5 for a given central atom. For the central atom La the values calculated by FEFF5 are: k_f = 1.6 Å^{-1}, E_f= 9.7 eV.

We calculated the radial distribution function $\rho(r)$ of the nearest Al neighbors to the central La atom by the RDF method [2] as follows:

$$\rho(r) = \frac{4}{\pi}\cdot\frac{r^2}{r_s^2}\int_0^\infty |\chi'|\sin(2kr_s + \Delta\Psi)\sin(2kr)dk. \quad (1)$$

$|\chi'(k)|$ and $\Delta\Psi(k)$ are the amplitudes ratio and phase difference of the unknown and standard data sets, respectively. r_s is the mean interatomic distance in the standard data structure. To calculate the integral in Eq. (1) we used the cumulant expansion to extrapolate the signal to $k = 0$. To reduce the cutoff wiggles from the upper limit of the data range, k_2, we employed the Gaussian factor $\exp(-2k^2\sigma_c^2)$. As a standard we used a theoretical XAFS signal generated by an individual photoelectron single scattering path La → Al with a half path length r_s, calculated with FEFF5. We determined r_s from the fit of the sum of FEFF5 paths between the central La and its different Al neighbors to the crystalline La_3Al_{11} XAFS data, where the distribution of atoms is

known [5]. The fit of the theoretical χ to the crystal data was performed in r-space, using the program FEFFIT (Univ. of Wash.). To isolate the first shell the r range from 2.0 Å to 4.0 Å was chosen. The range was limited from the higher r by the presence of the more distant La neighbors in the crystal. The unknown crystal data $\chi_u(r)$ and the standard $\chi_s(r)$ were then back Fourier transformed to k space and their ratio $\chi_u'(k)$ was obtained. The Gaussian factor 0.015 Å^2 was used to decrease the Fourier transform k_2 cutoff wiggles. Since the crystal structure is known, a theoretical $\chi_{th}'(k)$ was calculated straightforward, assuming that all 9 paths to Al atoms within the first shell have the same scattering amplitude and phase shifts. The coordination numbers, defined as the area below the RDF curves, are equal to 16.0 ± 0.2 for the model calculation $\chi_{th}'(k)$ and the experimental crystal data $\chi_u'(k)$. The centroid of $\rho(r)$ is at 3.32 ± 0.30 Å.

Changing a convergence factor gradually from 0.015 Å^2 to zero we resolved more and more structure for the crystal data. We found that the convergence factor affected the shape and the width of the distribution $\rho_{th}(r)$ dramatically. To demonstrate the splitting into subshells in the theoretical RDF and to avoid the cutoff wiggles we expanded an analytical $\chi_{th}'(k)$ far away in k space (up to 50 Å^{-1}) where no convergence factor was needed. The required vanishing of $\chi_{th}'(k)$ is provided by thermal DWF only. The spatial resolution is 0.01 Å.

The agreement between theory and data is good, verifying the accuracy of applying this method to the glass $Al_{0.91}La_{0.09}$. The RDF was obtained the same way as for the crystal. Calculations of the coordination number and the average La-Al distance over the shell gave the following results: N=14.45 ± 0.10, $\langle R_{La\text{-}Al} \rangle = 3.33 \pm 0.05$ Å.

To study how the convergence factor affects the RDF of the glass we varied it from 0.015 Å^2 to 0 and compared the resultant RDFs. It turned out that the RDFs look similar and almost no change in the broadening may be noticed, in contrast to the crystal. Now, comparing the two RDFs for the glass and the crystal we conclude that the distribution of atoms in the glass shows some shorter bonds than the crystal allows below 3.16 Å. Evaluating the number of atoms contained in the glass within the distances below 3.16 Å (the distance to the left wing of the RDF for crystal, Fig. 1.) we find $N = 1.7 \pm 0.1$, giving the mean number of the short bonds in the glass. The mean short bond length is found to be 3.09 ± 0.05 Å.

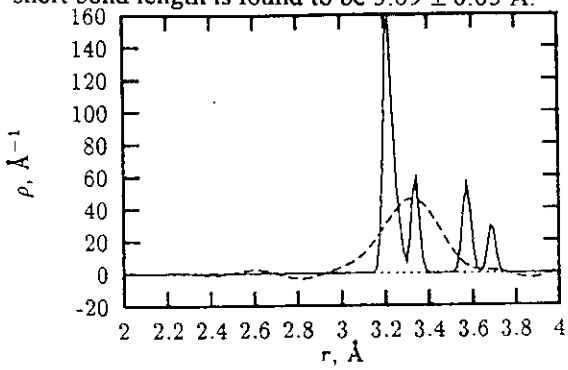

Fig. 1. RDF for the glass $Al_{0.91}La_{0.09}$ (dash) and the theory for crystal La_3Al_{11} (solid).

In conclusion we find a large change in $\rho(r)$ between the glass and the phase that crystallizes from it. The glass $\rho(r)$ shows some bonds shorter than found in the crystalline phase. It is suggested that this shortening is important in understanding the unusual properties of the $Al_{0.91}La_{0.09}$ glass, including its formation at such low La concentrations.

The calculation of the radial distribution functions was performed using the program RDF. This work was supported in part by the US - Israel BSF Grant No. 90-00152/1 and by the DOE Grant No. DE-FG06-90ER45425.

References

[1] A.Rubshtein, Y.Rosenberg, A.Frenkel, V.Manov, E.Veljulin, and A.Voronel, Report at the ISMANAM-94, Grenoble, 1994.

[2] E.A.Stern, Y.Ma, O.Hanske-Petitpierre, and C.E.Bouldin, Phys. Rev. B 46, 687 (1992).

[3] M.Newville, P.Livins, Y.Yacoby, J.J.Rehr, and E.A.Stern, Phys. Rev. B 47, 14126 (1993).

[4] J.J.Rehr, R.C.Albers, and S.I.Zabinsky, Phys. Rev. Lett. 69, 3397 (1992); J.Mustre de Leon, J.J.Rehr, S.I.Zabinsky, and R.C.Albers, Phys. Rev. B 44, 4146 (1991).

[5] A.H.Gomes de Mesquita and K.H.J. Buschow, Acta Cryst., 22, 497 (1967).

PHYSICAL REVIEW B VOLUME 49, NUMBER 17 1 MAY 1994-I

Solving the structure of disordered mixed salts

A. Frenkel
School of Physics and Astronomy, Raymond and Beverly Sackler Faculty of Exact Sciences, Tel Aviv University, Ramat Aviv 69978, Israel

E. A. Stern
Department of Physics FM-15, University of Washington, Seattle, Washington 98195

A. Voronel
School of Physics and Astronomy, Raymond and Beverly Sackler Faculty of Exact Sciences, Tel Aviv University, Ramat Aviv 69978, Israel

M. Qian
Princeton Materials Institute, Princeton, New Jersey 08540

M. Newville
Department of Physics FM-15, University of Washington, Seattle, Washington 98195
(Received 29 December 1993)

A detailed x-ray-absorption fine-structure (XAFS) investigation of two mixed alkali halides $Rb_{0.76}K_{0.24}Br$ and $RbBr_{0.62}Cl_{0.38}$ was performed. The concentrations of the mixtures had been chosen to produce a single homogeneous phase for each, and it was checked by XAFS that the salts were randomly mixed on the atomic level. Detailed analysis of the data including multiple-scattering contributions revealed an rms buckling angular deviation of both mixtures from the average NaCl collinear structure of 7–9°. The angles are defined by three atomic positions determined through double- and triple-scattering paths. These angles are new parameters which should be added to characterize the buckled crystals. Adding to diffraction results the parameters determined from XAFS as input into a molecular-dynamics simulation the structures of the mixed salts with their fluctuations about the NaCl structure are solved and displayed.

I. INTRODUCTION

The structure of solids is determined mainly by diffraction. For pure elements and compounds where the atoms are arranged in an ordered array, the sharp diffraction Bragg peaks give enough information to solve the structure. When elements and/or compounds are alloyed or mixed together, producing a single phase, the resultant solid still generally diffracts Bragg peaks, but in this case the Bragg reflections determine only the average structure, leaving unsolved the actual atomic deviation about this average. Typically the average structure has lattice constants[1] which approximately vary with composition x according to the virtual crystal approximation (VCA). The VCA states that the lattice constants approximately satisfy the Vegard's law of a linear interpolation between the corresponding pure components lattice constants, a_1 and a_2:

$$a_{\mathrm{mix}} = xa_1 + (1-x)a_2. \quad (1)$$

The Bragg diffraction in such mixtures indicates that the *average* structure of these materials is still periodic. In this paper we address the question of determining the *local* structure and the specific character of its deviation from the average, which gives a complete solution to the structure. The method of how this is done using the x-ray-absorption fine-structure (XAFS) technique has previously been outlined,[2] and in this paper we give further details and more results.

XAFS measurements in general imply that, locally, the atoms do not reside on the periodic structure. Indeed, it has been shown by XAFS in a variety of cases[3–7] that the actual nearest neighbor distances in alloys and mixed salts are different from the average distances calculated from the lattice constant assuming a perfect periodic lattice. Thus it is clear that, generally speaking, the atoms are not sitting on their lattice sites of the *average* structure, but it has never been defined what is the actual structure *locally* and how to determine it quantitatively. In this paper our goal is to define in detail and to visualize the local structure of the two analogous systems of mixed salts, $Rb_xK_{1-x}Br$ and $RbBr_xCl_{1-x}$, by thorough analysis of their XAFS data. This choice of samples is not incidental. While the crystalline symmetries of these two mixtures are similar and the size difference between randomized K and Rb ions is roughly equal to that between Cl and Br (≈ 0.15 Å),[8] and consequently their phase diagrams[8,9] are similar, the absolute sizes of the randomized atoms are quite different. Since the randomized atoms also have different charges, it is not obvious

0163-1829/94/49(17)/11662(13)/$06.00

that their local structure deviations will be similar.

The knowledge of the actual locations of atoms in disordered solids and the character of their deviation from the average structure is necessary for detailed understanding of their properties. The dielectric,[10] optical, electrical as well as mechanical properties[11] of single-phase mixed salts are expected to depend on the character of distortion of the perfect structure. It has recently been pointed out that also the melting of such disorderly alloyed solids depends on deviation from the perfect structure. The larger is the initial deviation from the perfect structure, the more it depresses the melting point.[8,12]

In our analysis of XAFS data we utilize the theoretical program[13] FEFF5 which includes multiple-scattering contributions to XAFS on a path by path basis. In particular we are able to estimate three-body correlations, which go beyond the usual two-body correlations normally taken into account by other means. The accuracy and power of FEFF5 have been demonstrated in describing the structure of the pure salts[14] RbBr, RbCl, KBr, constituting the elements of both of the series of mixtures chosen for our study. The reliability of FEFF5 has also been proven by its determining various distortions in several perovskites in close agreement with diffraction results.[10,15]

An outline of the paper is as follows. In Sec. II the experimental details are presented. The data analysis is discussed in Sec. III. Section IV discusses details of composition analysis. Structural characteristics of the mixed salts under consideration obtained within ≈ 8 Å around the central atom are presented in Sec. V. Results of molecular-dynamics simulations are discussed in Sec. VI. A general discussion of results is presented in Sec. VII and a summary and conclusion are presented in Sec. VIII.

II. EXPERIMENT AND SAMPLE PREPARATION

The reasons for our choice of the systems $Rb_xK_{1-x}Br$ and $RbBr_xCl_{1-x}$ are as follows. First, two (Rb, Br) of the three constituent elements of the mixtures have convenient K edge energies ($E_0 = 15240$ eV and 13500 eV, respectively) for XAFS measurements. Second, both systems are fully soluble in their solid states as shown in their phase diagrams[2] with the minimal points of congruent melting where liquid and solid are in equilibrium at one concentration at 24% KBr in the first and 38% RbCl in the second mixture.[8,9] This is the only assured condition to get a homogeneous solution in the bulk solid phase after freezing from the liquid, without additional annealing procedures. Any other composition typically crystallizes over a range of concentrations defined by the phase diagram and a cooling rate. Third, both systems have their consolute points (where they may theoretically separate into two solid phases) at rather low temperature[9] (120 K for the first and 119 K for the second mixture) where the rate of mutual diffusion within the mixtures is negligibly small and one should not expect a phase separation occurring during the low temperature XAFS measurements. Indeed, our thermal cycling around these points revealed no trace of the irreproducibility expected for the phase separation.

As described in Ref. 14, high purity (better than 99.9%) powders of raw materials of RbBr, KBr, and RbCl were supplied by Alfa (Johnson & Matthey). Two samples of mechanically mixed powders of above mentioned concentrations ($Rb_{0.76}K_{0.24}Br$ and $RbBr_{0.62}Cl_{0.38}$), corresponding to their respective minimum melting temperature compositions, were prepared from these raw materials. Each of them was carefully mixed, placed into a quartz ampule, heated to 120 °C for at least 1 h under vacuum of 10^{-3} Torr (to remove any trace of moisture since these salts are highly hygroscopic), and sealed off. Then the sealed ampules with the samples were transferred to a furnace and heated to 750 °C (higher than the melting points of all of the three pure components) for 48 h to homogenize the solutions. They were then quenched into cold water to solidification and annealed afterwards during 4 days at the temperature 600 °C (below the minimal melting points of the mixtures). The resultant mixed salts were bulk crystals with a lot of cracks and boundary lines. Finally these samples were removed from the quartz containers, ground to fine powders, sieved through 400 mesh, and rubbed as single layers onto Scotch tape and then sealed as a stacked array of layers in a vacuum tight cell, all within a dry glovebox.

To avoid a sample thickness effect[16] the following condition should be satisfied (for concentrated materials):

$$\Delta\mu d \ll 1, \quad \Delta\mu x < 1.5 , \tag{2}$$

where $\Delta\mu$ is the absorption edge step, d is the average grain size, and x is the sample thickness. The thicknesses corresponding to $\Delta\mu x = 1$ for $Rb_{0.76}K_{0.24}Br$ and $RbBr_{0.62}Cl_{0.38}$ at the Rb (Br) K edge are 67 (48) and 56 (78) μm, respectively. To obtain samples with total $\Delta\mu x \approx 1$ required stacking at least 14 layers of the powdered tape. Thus the average grain size of the salts ($d \approx 4$ μm) was small enough to assure a negligible thickness effect.

The XAFS measurements were performed on the beam line X-11A at the National Synchrotron Light Source (NSLS) with a double-crystal (111) silicon monochromator. Harmonics were attenuated to negligible levels by detuning the monochromator to 80% of its peak. Due to the large thermal disorder of the investigated materials, the measurements had to be performed at low temperature and only the 30 K and 125 K data that had been measured were analyzed.

III. DATA ANALYSIS

The experimental XAFS data on mixed salts $Rb_{0.76}K_{0.24}Br$ and $RbBr_{0.62}Cl_{0.38}$ at the congruent melting minimum points were analyzed in detail. The method of Ref. 17 was used to subtract the background function and obtain a normalized absorption function $\chi(k)$:

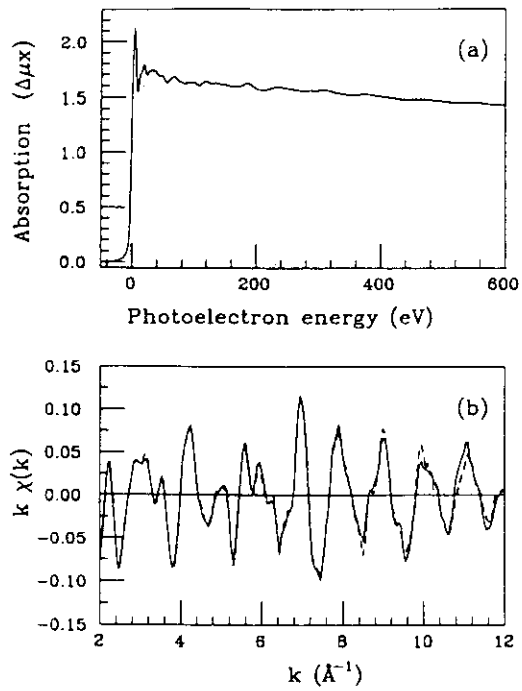

FIG. 1. (a) Absorption coefficient $\mu(E)x$, and (b) normalized absorption $\chi(k)$ at 30 K of two independent measurements (dashed and solid lines) of the Br edge of $Rb_{0.76}K_{0.24}Br$.

$$\chi(k) = \frac{\mu(k) - \mu_0(k)}{\Delta\mu_0(0)}, \tag{3}$$

where $k = \sqrt{2m(E - E_0)}$ is the wave number, E is the photon energy, $\mu(k)$ is the measured absorption, $\mu_0(k)$ is the background, and $\Delta\mu_0(0)$ is the edge jump. The $\Delta\mu(E)x$ data and resultant $\chi(k)$ of two independent measurements of $Rb_{0.76}K_{0.24}Br$ (Br edge) are shown in Fig. 1. The XAFS data were then fit to theoretical calculations,[13] as discussed below. The fits were done in R space, allowing shells higher than the first with their attendent multiple scattering to be correctly included in an organized way.

The reliability of multiple-scattering (MS) XAFS theory,[13] the computer code FEFF5, and the fitting procedure used has been demonstrated before[14] for the pure constituent compounds RbCl, KBr, and RbBr. In the pure salts, it was possible to obtain good fits up to 10 Å from the center atoms. However, to do so it was necessary to compensate for approximations in the theory by adding a small ΔE_0 shift to the potential seen by near neighbors.

In this work the structure of mixed salts was determined using the same analysis procedure and the same scattering paths found to be important for XAFS of the pure salts RbBr, RbCl, and KBr. Because the structures of the mixed salts are more disordered, the analyses could not be extended past 8.5 Å for the ordered sublattice atoms, namely, the Br edge of $Rb_{0.76}K_{0.24}Br$ and the Rb edge of $RbBr_{0.62}Cl_{0.38}$. For the disordered sublattice atoms, namely, the Rb edge of $Rb_{0.76}K_{0.24}Br$ and the Br edge of $RbBr_{0.62}Cl_{0.38}$, the structure could not be reliably determined past 5.5 Å. Use of XAFS to investigate the structure of mixed salts was done previously,[3–7] but only for the first nearest neighbor distributions.

The number of parameters P which may be determined in XAFS analysis is limited to be less than the number of independent data points in the spectrum, N, given by[18]

$$N = \frac{2}{\pi}\delta k \delta R + 2, \tag{4}$$

where δk and δR are, respectively, the ranges in k and R space over which the data are fit. The relevant quantities to determine N, such as δk, δR, and the Fourier transform window margins in k space over which the data range δk is gradually decreased to zero, the resultant N, and the subsequent P values for all investigated mixtures are listed in Table I as is the k^w factor which $\chi(k)$ is weighted with when fitting.

To best fit the data, three parameters for each important scattering path in the theory were allowed to vary. These adjustable parameters for each path were (1) ΔE_0 (shift of the photoelectron energy origin), (2) ΔR (the shift of the atom from its site in the pure salt), and (3) σ^2 (Debye-Waller factor or second cumulant[20]). An additional parameter, S_0^2 (the passive electron reduction factor for the central atom),[19] was fixed to be the same as that found for the pure salt[14] for each of the two central atoms, namely, 0.98 for Rb and 0.91 for Br. Because of geometric restrictions between scattering paths, some constraints could be placed on the variables, reducing the number of free parameters, P, in the fit.

Uncertainties in the P free variables were determined by requiring the statistic $\Delta\chi^2$ for each fit to increase by 1 from the best-fit value, where $\Delta\chi^2$ is defined as[21]

$$\Delta\chi^2 = \frac{N}{n}\sum_{i=1}^{n}\left(\frac{\chi_{\text{data}}(R_i) - \chi_{\text{theory}}(R_i)}{\delta_i}\right)^2. \tag{5}$$

TABLE I. Parameters of Fourier transform δk, δR, weighing parameter k^w, window margins dk_1 and dk_2, numbers of independent data points, N, and fit variables P used in $Rb_{0.76}K_{0.24}Br$ and $RbBr_{0.62}Cl_{0.38}$ data analysis.

Data	Edge	δk (Å^{-1})	δR (Å)	k^w	dk_1 (Å^{-1})	dk_2 (Å^{-1})	N	P
$Rb_{0.76}K_{0.24}Br$	Br	3–11	2–8.5	k	1.8	3	34	24
$Rb_{0.76}K_{0.24}Br$	Rb	3–10	2–5.5	k	1.5	3	16	9
$RbBr_{0.62}Cl_{0.38}$	Br	2.5–10	2–5.5	k	1.2	3	18	9
$RbBr_{0.62}Cl_{0.38}$	Rb	2.5–11	2–8.5	k	1.5	1.5	36	25

Here N is the number of independent data points [Eq. (4)], $\chi(R_i)$ is the Fourier transform of $\chi(k)$ at the point R_i, n is the number of points used to evaluate $\chi(R_i)$ (including both real and imaginary parts) over the range δR, and δ_i^2 is the sum of squares of the measurement uncertainty in $\chi_{\rm data}(R_i)$ and the systematic uncertainties. In the cases considered here, the measurement uncertainty was very small and δ_i was determined mainly by systematic uncertainties of background subtraction and the approximations made in the theory of FEFF5. The total systematic uncertainty was determined by requiring $\Delta\chi^2$ to be equal to $N-P$, as specified by statistical theory.[21] Correlations between the fit variables were taken into account when evaluating the uncertainties, so that the uncertainty in a parameter is the value by which that parameter must be changed in order to increase $\Delta\chi^2$ by 1 when all other parameters are optimized. All uncertainties are indicated in the tables in parentheses.

IV. COMPOSITION AND BOND LENGTH ANALYSIS

Consider the mixture $A_xB_{1-x}C$ of the salts AC and BC with composition x, and choose C to be an absorbing atom. One has to perform a fit of the theoretical $\chi(k)$ to the unknown structure data. X-ray diffraction results show that the average structure of such a mixture remains a NaCl type and, hence, one may use for fitting only those paths which have been found important for the analysis of the pure components.[14] The low R region ($2\,\text{Å} < r < 5.5\,\text{Å}$) is dominated by contributions from the two nearest shells. It includes three kinds of single-scattering (SS) paths, two corresponding to the two different first nearest neighbor (1NN) A or B atoms ($c \rightarrow 1\text{NN} \rightarrow c$, where c is the center atom, which is a C atom in this case) and one corresponding to the second nearest neighbor (2NN) distances C-C ($c \rightarrow 2\text{NN} \rightarrow c$).

The first shell XAFS, $\chi_{C1}(k)$, is simply the average of the contributions of the two respective scatterings $\chi_{CAC}(k)$ and $\chi_{CBC}(k)$,

$$\chi_{C1}(k) = y\chi_{CAC}(k) + (1-y)\chi_{CBC}(k), \qquad (6)$$

where the composition factor y is to be determined from the best fit of Eq. (6) to data. The resultant average y value should be always x, regardless of the degree of randomness of the distribution of components since both the homogeneous mixture and heterogeneous separated structure (and any combination in between) should produce an XAFS signal averaged over the total number of absorbers C, with contributions x and $1-x$ of the components CA and CB, respectively. The fitting of the 1NN paths to data was performed in accordance with Eq. (6). Indeed, the value of y found agreed with x within uncertainties (Table II) for both samples. It was also found that the A-C and B-C bond lengths $R_{\rm mix}$ in both mixtures (Tables III, IV) did not follow Vegard's law [Eq. (1)]; i.e., they are not equal to one another and the VCA value, though sometimes the difference is barely outside of the uncertainties.

TABLE II. Comparison of concentration x and composition factor y as determined from fits to the 1NN of C and to the 2NN of A atoms in $A_xB_{1-x}C$. Superscripts indicate the coordination shell.

$A_xB_{1-x}C$	Bond	x	y
$Rb_{0.76}K_{0.24}Br$	Br-Rb[1]	0.76	0.76(1)
	Rb-Rb[2]	0.76	0.76(1)
$RbBr_{0.62}Cl_{0.38}$	Rb-Br[1]	0.62	0.62(1)
	Br-Br[2]	0.62	0.61(1)

To find out the degree of randomness of the distribution realized in the mixture $A_xB_{1-x}C$ one needs to go to the 2NN and to investigate the A or B edge XAFS of this mixture. Now, if full phase separation occurs, the 2NN to an A atom should be another A atom with 100% probability. However, for the opposite case of a fully random mixture the second neighbor to an A atom will be either again an A or a B atom in the ratio of x to $1-x$. Hence, it is straightforward to determine the degree of randomness from the y value found from the best fit to data of the $\chi_{A2}(k)$ of the 2NN paths:

$$\chi_{A2}(k) = y\chi_{AAA}(k) + (1-y)\chi_{ABA}(k), \qquad (7)$$

where χ_{AAA} is the contribution for A being both center and 2NN atoms, and χ_{ABA} is the contribution for A being the center and B the 2NN. Our previous analysis of the pure materials showed that only the SS paths give significant contributions to the 2NN peak.

The mixed sublattice atoms were analyzed, namely, the Rb edge data of $Rb_{0.76}K_{0.24}Br$ and the Br edge data of $RbBr_{0.62}Cl_{0.38}$. The fitting of the 2NN paths Rb $\rightarrow$ Rb and Rb $\rightarrow$ K $\rightarrow$ Rb to the second peak of the $Rb_{0.76}K_{0.24}Br$ (Rb edge) data [Fig. 2(a) and Table II] gave $y = 0.76 \pm 0.01$, demonstrating that complete

TABLE III. Four nearest bond lengths (in Å) about Br edge in pure RbBr, KBr, and $Rb_{0.76}K_{0.24}Br$, and VCA values (Ref. 1). Superscripts indicate the coordination shell. The row with brackets gives the distance averaged over composition.

	Br-K[1]	Br-Rb[1]	Br-Br[2]	Br-K[3]	Br-Rb[3]	Br-Br[4]
RbBr	—	3.410(10)	4.822(10)	—	5.906(10)	6.820(10)
KBr	3.270(10)	—	4.624(10)	5.664(10)	—	6.540(10)
$Rb_{0.76}K_{0.24}Br$	3.361(15)	3.393(10)	4.761(10)	5.860(20)	5.890(20)	6.743(15)
$\langle Rb_{0.76}K_{0.24}Br\rangle$	3.385(11)	3.385(11)	4.761(10)	5.883(20)	5.883(20)	6.743(15)
VCA	3.378	3.378	4.777	5.850	5.850	6.755

TABLE IV. Four nearest bond lengths (in Å) about Rb edge in pure RbBr, RbCl, and $RbBr_{0.62}Cl_{0.38}$, and VCA values (Ref. 1). Superscripts indicate the coordination shell. The row with the brackets gives the distance averaged over composition.

	Rb-Cl[1]	Rb-Br[1]	Rb-Rb[2]	Rb-Cl[3]	Rb-Br[3]	Rb-Rb[4]
RbBr	—	3.410(10)	4.822(10)	—	5.906(10)	6.820(10)
RbCl	3.270(10)	—	4.624(10)	5.664(10)	—	6.540(10)
$RbBr_{0.62}Cl_{0.38}$	3.336(15)	3.383(10)	4.753(10)	5.760(20)	5.810(20)	6.710(15)
$\langle RbBr_{0.62}Cl_{0.38}\rangle$	3.365(12)	3.365(12)	4.753(10)	5.791(20)	5.791(20)	6.710(15)
VCA	3.357	3.357	4.747	5.814	5.814	6.713

random solubility occurred in the mixture preparation and therefore our following results in the larger R range, which assume this randomness, are trustworthy.

The first peak in R space of the $Rb_{0.76}K_{0.24}Br$ χ function [Fig. 2(a)] was fit by the single-scattering 1NN path Rb-Br-Rb with the half path length 3.39 Å which is only 0.02 ± 0.015 Å shorter than that of pure RbBr (Table V). A similar analysis about the Br edge gave the same value for the Br-Rb nearest neighbor distance (Table III), as it should. This shortening of the first peak suggests that the first nearest neighbors bond length of pure salt may not be conserved in the mixture, in agreement with the results obtained in Refs. 3–7, but the difference for Br-Rb is too close to the uncertainty to be definitive. However, the analysis of the low-R-range data for the Br edge of the same mixed salt determined the Br-K 1NN distance to be 0.091 ± 0.015 Å longer than in pure KBr (Table III), distinctively different from the Br-Rb bond

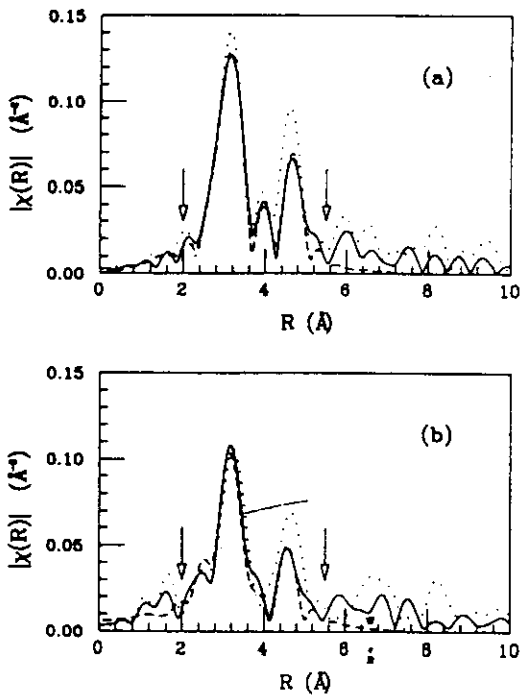

FIG. 2. $\chi(R)$ of (a) Rb edge data of $Rb_{0.76}K_{0.24}Br$ (solid line), pure RbBr (dotted line), and fit to the mixture (dashed line); (b) Br edge data of $RbBr_{0.62}Cl_{0.38}$ (solid line), pure RbBr (dotted line), and fit to the mixture (dashed line). The range over which the fit has been made is shown by the arrows. All the data are taken at $T = 30$ K.

length change. Thus a first neighbor distance changes asymmetrically with concentration.

The same analysis was performed for the Br edge data of the other investigated mixture, $RbBr_{0.62}Cl_{0.38}$ [Fig. 2(b) and Table II] and the composition parameter of the components RbBr and RbCl was again determined from the fit to the second peak in R space by the 2NN SS paths Br → Br → Br and Br → Cl → Br. The obtained value $y = 0.61 \pm 0.01$ shows again that the components in the minimal melting point are randomly mixed with the desired concentration and the 1NN Rb-Br bond length (3.383 Å) also exhibited a small shift ($\Delta R = -0.027 \pm 0.010$ Å) relative to the pure RbBr bond length (Table VI). The same value of this bond length was obtained by analyzing the Rb edge data (Table IV). Here again the shift is still close to uncertainty to be definitive. However, analysis of the first peak in R space of the Rb edge for the same mixed salt gives a 0.066 ± 0.015 Å shift towards larger R in the Rb-Cl 1NN distance with respect to the pure RbCl (Table IV). Thus the shorter bond again changes dramatically in the mixture.

In the fits above we varied the shift of the photoelectron energy origin ΔE_0 for each of the three considered paths independently (one 1NN and two 2NN SS paths for the mixed atom as the center atom, and two 1NN and one 2NN SS paths for the common atom as the center one). In the previous work[14] on the pure salts it was shown that the paths containing first nearest neighbors must have an additional ΔE_1 shift to the ΔE_0 overall of all the other SS paths, which was interpreted as being caused by the lack of complete shielding of the core hole potential at the 1NN. The mixed salts indicate that a similar correction to FEFF5 is required for them also.

Analyzing the C-C (2NN) distances we found that in both $Rb_{0.76}K_{0.24}Br$ and $RbBr_{0.62}Cl_{0.38}$ Vegard's law was valid within uncertainties for the lengths of Br-Br and Rb-Rb separations, respectively (Tables III, IV). These

TABLE V. Two nearest bond lengths (in Å) about Rb edge in pure RbBr, and $Rb_{0.76}K_{0.24}Br$, and VCA values (Ref. 1). Superscripts indicate the coordination shell. The row with brackets gives the distance averaged over composition.

	Rb-Br[1]	Rb-K[2]	Rb-Rb[2]
RbBr	3.410(10)	—	4.822(10)
$Rb_{0.76}K_{0.24}Br$	3.390(10)	4.800(15)	4.790(15)
$\langle Rb_{0.76}K_{0.24}Br\rangle$	3.390(10)	4.792(15)	4.792(15)
VCA	3.378	4.777	4.777

TABLE VI. Two nearest bond lengths (in Å) about Br edge in pure RbBr, and $RbBr_{0.62}Cl_{0.38}$, and VCA values (Ref. 1). Superscripts indicate the coordination shell. The row with brackets gives the distance averaged over composition.

	Br-Rb[1]	Br-Cl[2]	Br-Br[2]
RbBr	3.410(10)	—	4.822(10)
$RbBr_{0.62}Cl_{0.38}$	3.390(10)	4.710(15)	4.710(15)
$\langle RbBr_{0.62}Cl_{0.38}\rangle$	3.390(10)	4.710(15)	4.710(15)
VCA	3.357	4.747	4.747

distances are identical to lattice constants defined by x-ray diffraction for these salts[1] and do closely follow Vegard's law. The violation of Vegard's law for the 1NN bonds and its concurrent validity for the 2NN bonds lead to buckling of the bonds as discussed in Sec. V.

V. MULTIPLE SCATTERINGS AND DEVIATIONS FROM COLLINEARITY

Once the homogeneity and randomness of the mixtures $A_xB_{1-x}C$ are verified, one can analyze the structure in the more distant R range which includes multiple scatterings. Our analysis was performed with the C edge data in both mixtures. This is the first time to our knowledge that the analysis of mixed salts beyond the first shell has been undertaken with an accurate account of multiple-scattering effects.

To extend the fitting procedure to the more distant R range, starting with the third nearest neighbor (3NN) distance, one should properly treat the single-scattering (SS) and multiple-scattering (MS) paths, contributing to this range. The variables should be carefully chosen in the fitting procedure so as to limit their number to the minimum required. Thus, we need to decrease the number of paths involved to only those that give significant contributions and to account for all correlations between the various parameters.[14] As shown in Ref. 14 the most important paths needed for the analysis of salts with NaCl structure are single-scattering (SS), double-scattering (DS), and triple-scattering (TS) collinear paths. We, therefore, in the present work deal with such paths only.

The shortest paths beyond 2NN are SS paths $c \rightarrow$ 3NN $\rightarrow c$, corresponding to the pairs Br-Rb, Br-K for the Br edge of $Rb_{0.76}K_{0.24}Br$ data and Rb-Br, Rb-Cl for the Rb edge of $RbBr_{0.62}Cl_{0.38}$ data. There are two fit variables assigned to each of the paths: ΔR and σ^2. We fix the energy origin shift of these paths to be equal to the ΔE_0 overall found for the 2NN bond Br-Br (Rb-Rb) and the composition parameter $y = x$ as found in the previous section.

The next SS path connects the absorber and the fourth nearest neighbor (4NN). Again, we varied ΔR as well as σ^2. There are four more paths to the 4NN in our analysis with the same half path length as the SS path which were fit to the data simultaneously since all of them contribute to the same R range 5–7 Å. They are double (DS) and triple-scattering (TS) focusing paths:[14] $c \rightarrow$ 1NN $\rightarrow$ 4NN $\rightarrow c$ (and its time reverse) and $c \rightarrow$ 1NN $\rightarrow$ 4NN $\rightarrow$ 1NN $\rightarrow c$, respectively. Each of these paths has two different contributions from the two different 1NN intervening atoms. Using the notation $A_xB_{1-x}C$ for the mixed salts, we can denote these paths as follows. Absorber is C, backscatterer C', focusing atom A: $C \rightarrow A \rightarrow C' \rightarrow C$ (DS) and its time reverse, and $C \rightarrow A \rightarrow C' \rightarrow A \rightarrow C$ (TS); focusing atom B: $C \rightarrow B \rightarrow C' \rightarrow C$ (DS), and its time reverse, and $C \rightarrow B \rightarrow C' \rightarrow B \rightarrow C$ (TS). In these cases the C' atom is a 4NN and the focusing atom is a 1NN. Figure 3 represents schematically examples of SS, DS, and TS paths. The DS and TS paths are called focusing because the forward scattering of the intervening atom enhances the total signal. There are two more kinds of SS paths to the 5NN and 6NN which contribute to the total $\chi(R)$ within R range 7–8 Å and were fit to data but they do not interfere with the shorter paths.[14]

Since it was found from the fitting results of the 1NN paths that bond lengths C-A and C-B are different, the A and B atoms must be off their average lattice sites, because in the average structure these two bond lengths are equal. It can be shown that this means that the DS and TS paths are no longer collinear, contrary to what they are in the perfect structure. Describing the deviation from collinearity of these paths in terms of buckling angles $\Theta_1 = 180° - \widehat{CAC'}$ and $\Theta_2 = 180° - \widehat{CBC'}$, one can add these two more parameters (Θ_1 and Θ_2) to focusing DS and TS paths and determine them from the fit.

A theoretical expression[13] of $\chi(k)$ of the MS path contains a product of scattering amplitudes F_i, where i denotes the atomic site. The forward-scattering amplitude F of the intervening (focusing) atom in these paths as a function of Θ has its maximum at collinearity (at $\Theta = 0$) (see Ref. 22), and since it is even in Θ, an expansion

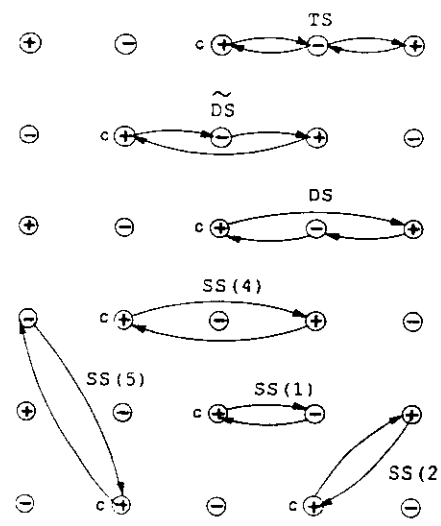

FIG. 3. Schematic of photoelectron SS(1), SS(2), SS(4), and SS(5) paths in the (100) plane of a NaCl structure to the 1NN, 2NN, 4NN, and 5NN, respectively, and DS (and its time reversed path $\tilde{\text{DS}}$) and TS paths to the 4NN. In all the cases the center atom is a positive ion denoted by c. SS paths to 3NN and 6NN are out of the plane.

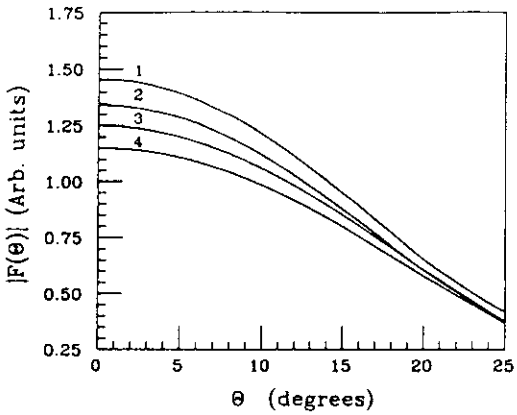

FIG. 4. $F(k,\Theta)$ ($k = 8\,\text{Å}^{-1}$) of nearly collinear DS paths: (1) Br-Rb^1-Br^4-Br; (2) Rb-Br^1-Rb^4-Rb; (3) Br-K^1-Br^4-Br; (4) Rb-Cl^1-Rb^4-Rb. Superscripts indicate the coordination shell.

of $F(k,\Theta)$ about $\Theta = 0$ has its lowest order of Θ^2. Averaging over the total number of absorbing atoms, one obtains

$$\langle F(k,\Theta)\rangle \approx F(k,0)[1 - b(k)\langle\Theta^2\rangle], \tag{8}$$

where the precisely forward-scattering amplitude of the intervening atom $F(k,0)$ is determined with that FEFF5 calculation which gives good agreement[14] with the ordered structure of the corresponding pure salts. The curvature coefficient $b(k)$ is obtained as follows. The $F(k,\Theta)$ is calculated with FEFF5 for the DS path described above with the focusing atom (the 1NN atom) moved out of its collinear site with varying Θ values. The $b(k)$ is then found by a fit to Eq. (8) in the small Θ range (up to 20°). The behavior of $F(k,\Theta)$ of the DS paths with Rb or Br as absorbers and Br, Cl or Rb, K as focusing atoms, respectively, for $k = 8\,\text{Å}^{-1}$ is shown

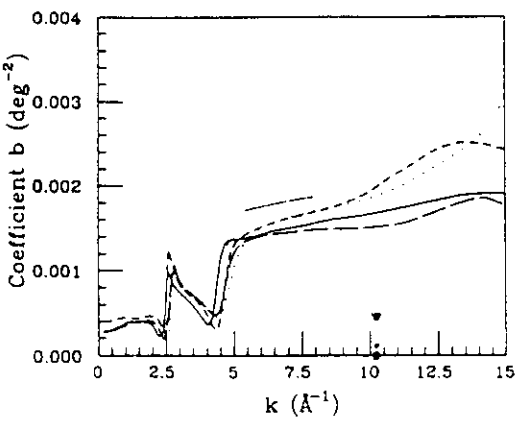

FIG. 5. Curvature coefficient $b(k)$ for the DS paths. Absorber Br with focusing atoms K (solid line) and Rb (dashed line), and absorber Rb with focusing atoms Br (dotted line) and Cl (long dashed line).

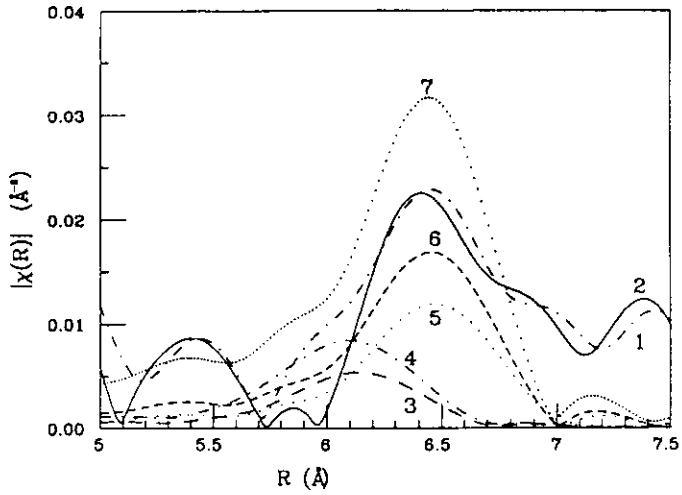

FIG. 6. Contributions of individual Θ-dependent paths to the total fit in R space for the Br edge data of $Rb_{0.76}K_{0.24}Br$ at 30 K. Denoted by numbers are (1) data; (2) fit; (3) DS paths Br-K^1-Br^4-Br and its time reverse; (4) TS path Br-K^1-Br^4-K^1-Br; (5) SS path Br-Br^4-Br; (6) DS paths Br-Rb^1-Br^4-Br and its time reverse; (7) TS path Br-Rb^1-Br^4-Rb^1-Br.

on Fig. 4. Figure 5 shows the calculated $b(k)$ dependence for these paths. Since the Fourier transform window range $k_{\min} = 2.5\,\text{Å}^{-1}$, $k_{\max} = 11\,\text{Å}^{-1}$ with margins $dk = 1.5\,\text{Å}^{-1}$ (Table I) correspond to the approximately flat region of $b(k) \approx 0.0018$ deg^{-2}, one can fix $b(k)$ to that constant and introduce the new fit variable $\langle\Theta^2\rangle$,

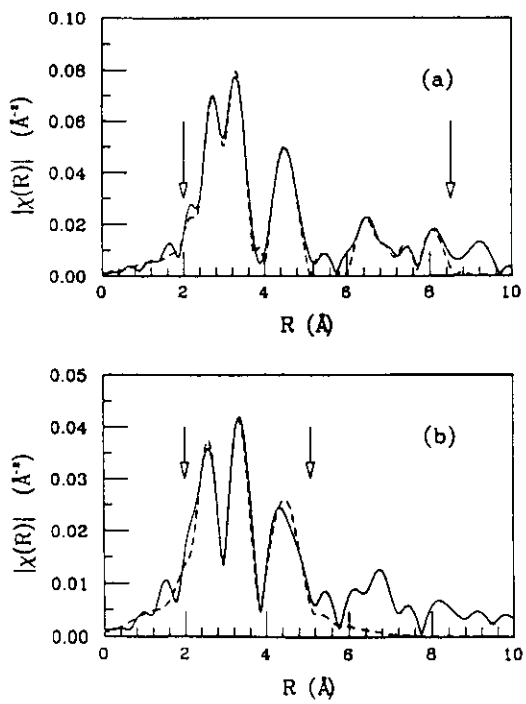

FIG. 7. Fit of the theoretical $\chi(R)$ (dashed line) to the Br edge data of $Rb_{0.76}K_{0.24}Br$ (solid line) at (a) 30 K and (b) 125 K. The range over which the fit has been made is shown by the arrows.

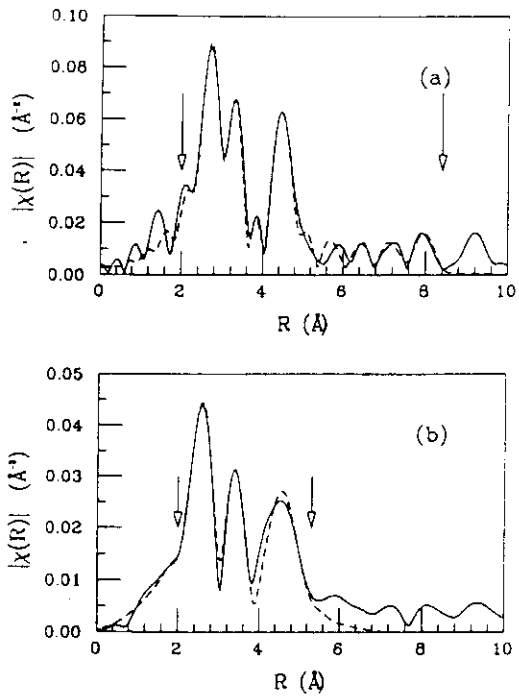

FIG. 8. Fit of the theoretical $\chi(R)$ (dashed line) to the Rb edge data of $RbBr_{0.62}Cl_{0.38}$ (solid line) at (a) 30 K and (b) 125 K. The range over which the fit has been made is shown by the arrows.

contributing to the amplitude of $\chi(k)$ as $(1-0.0018\langle\Theta^2\rangle)$.

The fit was performed in the R range 5–7 Å for both mixtures. The paths involved were the above described two kinds of SS paths ($c \rightarrow 3NN \rightarrow c$ and $c \rightarrow 4NN \rightarrow c$), two kinds of DS and TS paths. Figure 6 gives the contributions of different paths to the final fit in the corresponding R range. These DS and TS contributions are not small and therefore give us a real possibility to measure buckling angles.

Note that the TS path requires only one fitting variable additional to the DS paths, namely, a $\Delta E_0'$ shift: The focusing atom (1NN) scatters the photoelectron twice and the amplitude of $\chi(k)$ is multiplied by the factor $(1-0.0018\langle\Theta^2\rangle)^2$.

Another fit variable, ΔR of the TS path, differs generally from that of the corresponding DS path. However, in our case, where the difference in bond lengths AC and BC is relatively small, we expect the deviations from the average structure to be also small and the rms bond angles $\langle\Theta^2\rangle^{1/2}$ not to exceed 20°. Thus, the difference in the half path length of the DS and TS paths is expected not to exceed 0.015 Å, which is the uncertainty of the distance determination with XAFS (see Tables III, IV) and one can set $\Delta R_{DS} = \Delta R_{TS}$ to a good approximation. This also implies that the Debye-Waller factors of the DS and TS paths, connecting the central atom, focusing atom (1NN) and the 4NN atom are approximately equal to the σ^2 of the single pair $c-4NN$ due to the relation[14] $\sigma^2_{DS} = \sigma^2_{TS} = \sigma^2_{SS}$, verified to be valid in the analysis of pure salts.

The fit results up to $R = 8$ Å for both mixtures at 30 K are shown on Figs. 7(a) and 8(a). As a final check of our approximation of a constant b, we set the $\langle\Theta^2\rangle$ values to those found in our fit, and then calculated the XAFS spectrum using the $b(k)$ variable in k and obtained fits which were indistinguishable from the one obtained with the constant b. Figures 7(b) and 8(b) show fits to only the two nearest neighbors at 125 K ($Rb_{0.76}K_{0.24}Br$, Br edge, and $RbBr_{0.62}Cl_{0.38}$, Rb edge, respectively), in order to determine the 1NN temperature dependence of σ^2.

Values of fit variables including obtained bond angles are given in Tables VII, VIII. The rms deviations from collinearity actually are less than 10°, validating the approximations used.

TABLE VII. Path parameters ΔE_i (in eV) and σ_i^2 (in 10^{-2} Å^2) of $Rb_{0.76}K_{0.24}Br$ (Br edge) data at 30 K. DW factors of the 1NN paths at 125 K are given in brackets. σ_i^2 of pure salts (Ref. 14) RbBr and KBr (Br edge) are given for comparison. Superscripts indicate the coordination shell.

Path	ΔE_i	σ^2_{mix}	σ^2_{RbBr}	σ^2_{KBr}	Θ (deg)
$Br \rightarrow K^1 \rightarrow Br$	2.6(5)	0.64(5)	—	0.61(5)	—
		[1.4(1)]		[1.0(1)]	
$Br \rightarrow Rb^1 \rightarrow Br$	3.6(5)	0.60(5)	0.54(5)	—	—
		[1.1(1)]	[1.05(5)]		
$Br \rightarrow Br^2 \rightarrow Br$	0.8(5)	1.30(5)	0.73(5)	0.51(5)	—
$Br \rightarrow K^3 \rightarrow Br$	0.8(5)	1.62(5)	—	0.87(5)	—
$Br \rightarrow Rb^3 \rightarrow Br$	0.8(5)	1.36(5)	1.1(1)	—	—
$Br \rightarrow Br^4 \rightarrow Br$	0.8(5)	1.00(5)	0.77(5)	0.57(5)	—
$Br \rightarrow K^1 \rightarrow Br^4 \rightarrow Br$	0.0(5)	1.00(5)	—	0.57(5)	7.7(2.7)°
$Br \rightarrow Rb^1 \rightarrow Br^4 \rightarrow Br$	0.0(5)	1.00(5)	0.77(5)	—	9.0(1.6)°
$Br \rightarrow K^1 \rightarrow Br^4 \rightarrow K^1 \rightarrow Br$	-0.5(5)	1.00(5)	—	0.57(5)	7.7(2.7)°
$Br \rightarrow Rb^1 \rightarrow Br^4 \rightarrow Rb^1 \rightarrow Br$	-0.5(5)	1.00(5)	0.77(5)	—	9.0(1.6)°
$Br \rightarrow K^5 \rightarrow Br$	0.8(5)	1.2(1)	—	0.85(5)	—
$Br \rightarrow Rb^5 \rightarrow Br$	0.8(5)	1.4(1)	—	—	—
$Br \rightarrow Br^6 \rightarrow Br$	0.8(5)	1.45(10)	—	0.55(5)	—

TABLE VIII. Path parameters ΔE_i (in eV) and σ_i^2 (in 10^{-2} Å^2) of $RbBr_{0.62}Cl_{0.38}$ (Rb edge) data at 30 K. DW factors of the 1NN paths at 125 K are given in brackets. σ_i^2 of pure salts (Ref. 14) RbBr and RbCl (Rb edge) are given for comparison. Superscripts indicate the coordination shell.

Path	ΔE_i	σ_i^2	σ^2_{RbBr}	σ^2_{RbCl}	Θ (deg)
$Rb \rightarrow Cl^1 \rightarrow Rb$	1.3(5)	0.96(5)	—	0.55(5)	—
		[2.1(1)]		[1.07(5)]	
$Rb \rightarrow Br^1 \rightarrow Rb$	-1.3(5)	0.60(5)	0.55(5)	—	—
		[1.0(1)]	[1.05(5)]		
$Rb \rightarrow Rb^2 \rightarrow Rb$	-2.4(5)	1.27(5)	0.71(5)	0.40(5)	—
$Rb \rightarrow Cl^3 \rightarrow Rb$	-2.4(5)	1.40(5)	—	0.55(5)	—
$Rb \rightarrow Br^3 \rightarrow Rb$	-2.4(5)	1.50(5)	1.06(5)	—	—
$Rb \rightarrow Rb^4 \rightarrow Rb$	-2.4(5)	1.40(5)	0.81(5)	0.44(5)	—
$Rb \rightarrow Cl^1 \rightarrow Rb^4 \rightarrow Rb$	0.0(5)	1.40(5)	—	0.44(5)	7.3(3.0)°
$Rb \rightarrow Br^1 \rightarrow Rb^4 \rightarrow Rb$	0.0(5)	1.40(5)	0.81(5)	—	8.2(1.5)°
$Rb \rightarrow Cl^1 \rightarrow Rb^4 \rightarrow Cl^1 \rightarrow Rb$	-2.0(5)	1.40(5)	—	0.44(5)	7.3(3.0)°
$Rb \rightarrow Br^1 \rightarrow Rb^4 \rightarrow Br^1 \rightarrow Rb$	-2.0(5)	1.40(5)	0.81(5)	—	8.2(1.5)°
$Rb \rightarrow Cl^5 \rightarrow Rb$	-2.4(5)	0.98(5)	—	1.20(5)	—
$Rb \rightarrow Br^5 \rightarrow Rb$	-2.4(5)	1.9(1)	2.02(5)	—	—
$Rb \rightarrow Rb^6 \rightarrow Rb$	-2.4(5)	1.5(1)	1.0(1)	0.80(5)	—

VI. COMPUTER SIMULATION

Using the XAFS results for the average values, a model of the structure showing the distribution of bond lengths and bond angles of the mixed ionic salts under consideration may be calculated using the molecular-dynamics (MD) simulation method, in which the equations of lattice motion are integrated numerically. The atoms in ionic salts, especially alkali halides, have a high degree of charge transfer and their interatomic potentials consist of a sum of Coulomb and repulsion terms. The anharmonicity of the atomic vibrations are found to become significant only well above 30 K, and so at 30 K these potentials V may be approximated as harmonic,

$$V = \frac{1}{2}\sum_{i<j} k_{ij}(R_{ij} - \rho_{ij})^2, \tag{9}$$

where k_{ij} is the effective force constant, and R_{ij} and ρ_{ij} are the distances between the i and j ions and their equilibrium bond lengths, respectively. We add the approximation in Eq. (9) that the interactions are significant only between the first nearest neighbors. Therefore, in the case of the NaCl-type cubic lattice the summation is performed over the six nearest neighbor bonds.

We used in this work the simulation method[23] and computer code CLUSTER,[23] which showed good agreement with experiment for the simulation of pure alkali halides. The equations of motions were integrated in Ref. 23 using a fifth-order predictor-corrector algorithm.[24] The program CLUSTER was applied in our work to calculate the mixed salts with the interatomic potentials of Eq. (9), where i and j are the nearest neighbors, $\rho_{ij} = \rho_{AC}$ or ρ_{BC}, the average lengths of the bonds A-C or B-C, respectively, as determined here by XAFS, and k_{AC} and k_{BC} are the force constants of these bonds.

At low temperature, where zero point motion dominates, the force constants may be obtained from the Einstein formula[25] for the Debye-Waller factor:

$$\sigma^2 \cong \frac{\hbar}{2\mu\omega}, \tag{10}$$

where ω is the oscillation frequency of the pair and $\mu = (M_1^{-1} + M_2^{-1})^{-1}$ is its reduced mass. Finding ω from the values of σ^2 of the first nearest neighbor bonds, determined for pure salts,[14] one can calculate $k_{ij} = \mu\omega^2$. We assume that the k_{ij} determined from the pure salts are a good enough approximation for the mixed salt case. Our result is not sensitive to this approximation. Table IX contains the values of σ^2, μ, ω, and k_{ij} calculated for the Rb-Br, Rb-Cl, and K-Br bonds in the pure salts.

The simulation was performed over both $9 \times 9 \times 9$ (729 atoms) and $11 \times 11 \times 11$ (1331 atoms) clusters in order to check for surface effects. The initial configuration $A_xB_{1-x}C$ was prepared using a random number generator for placing A and B atoms at their sites in accordance with the concentration x. Atoms C were placed at the sites of the average lattice with the lattice parameter $a = 6.74$ Å for Br-Br (4NN) distance in $Rb_{0.76}K_{0.24}Br$ and $a = 6.71$ Å for Rb-Rb (4NN) distance in $RbBr_{0.62}Cl_{0.38}$, as determined from our XAFS analysis. The atoms A and B were initially placed in the middle of the C-C bond. In order to satisfy the fit results for the first path (Tables III, IV) we set $\rho_{AC} = \rho_{Rb\text{-}Br} = 3.39$ Å, $\rho_{BC} = \rho_{K\text{-}Br} = 3.36$ Å in $Rb_{0.76}K_{0.24}Br$ $\rho_{AC} = \rho_{Rb\text{-}Br} = 3.38$ Å, $\rho_{BC} = \rho_{Rb\text{-}Cl} = 3.34$ Å in $RbBr_{0.62}Cl_{0.38}$.

During the subsequent MD run the surface atoms were

TABLE IX. σ^2, reduced masses, Einstein frequencies, and force constants of Rb-Br, K-Br and Rb-Cl bonds in our computer simulations.

Bond	σ^2 (10^{-3} Å^2)	μ (10^{-27} kg)	ω (10^{13} Hz)	k_{ij} (N/m)
Rb-Br	5.5	68.6	1.4	13.4
K-Br	6.1	43.6	2.0	17.4
Rb-Cl	5.5	41.5	2.3	22.0

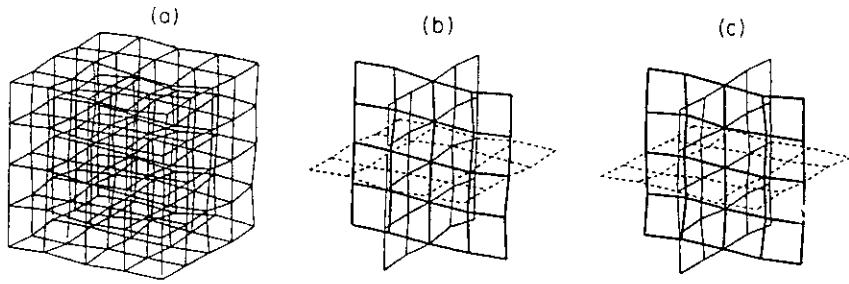

FIG. 9. Equilibrium cluster (inner 125 atoms) configurations: (a) $RbBr_{0.62}Cl_{0.38}$. To minimize overlap from the various bonds and atoms of (a), only the atoms comprising the center sections are shown in (b). (c) The atoms comprising the center sections of $Rb_{0.76}K_{0.24}Br$.

fixed by setting their velocities to zero. The internal atoms were allowed to move in accordance with equations of motion and initially given random velocities which were then rescaled several times in order to obtain a stable equilibrium configuration in the minimum of the potential well. The time step was chosen to be 10^{-15} sec [it must be at least an order of magnitude smaller than the bond oscillation period ω^{-1} (Table IX)]. For both clusters averaging was done only over the inner $5 \times 5 \times 5$ cluster to exclude the influence of the fixed surface atoms. For the larger cluster, averaging was also done over the inner $7 \times 7 \times 7$ cluster to verify that the averaged region had been immersed into the interior deeply enough to be insulated from surface effects. The time averaging (2×10^{-11} sec) was performed during the last run of the program where the desired equilibrium was achieved. The results for angles obtained from the various clusters agreed one with another to about 0.1°, indicating that surface effects were negligible.

The simulation results in equilibrium were found to be in excellent agreement with the XAFS results. The equilibrium bond lengths $\rho_{Rb\text{-}Br} = 3.39$ Å, $\rho_{K\text{-}Br} = 3.37$ Å, and $\rho_{Rb\text{-}Cl} = 3.34$ Å are consistent with those determined by XAFS within the uncertainty 0.01 Å. The rms bond angles found with MD simulation for the final configuration of atoms were Θ(Br-Rb-Br) = 8.2°, Θ(Br-K-Br) = 8.0° in $Rb_{0.76}K_{0.24}Br$ and Θ(Rb-Br-Rb) = 8.8°, Θ(Rb-Cl-Rb) = 8.0° in $RbBr_{0.62}Cl_{0.38}$, agreeing within uncertainties with the measurements (Tables VII, VIII). Figures 9(a) and 9(b) show the equilibrium configurations of $Rb_{0.76}K_{0.24}Br$ and $RbBr_{0.62}Cl_{0.38}$ clusters, respectively. The static distortions off NaCl structure sites are clearly seen on both plots. Within the uncertainties these pictures should be considered as actual structures of our mixed salts.

VII. DISCUSSION

Our XAFS results give microscopic local information on the structure of the two mixed salts $Rb_{0.76}K_{0.24}Br$ and $RbBr_{0.62}Cl_{0.38}$ which can hardly be obtained by other means. The distances between pairs of atoms, the three-body correlations expressed in terms of the buckling angles from collinearity, the relative amplitudes of vibration of the atoms, and the evidence that their two component salts are randomly mixed were derived from XAFS. This microscopic local information determines the detailed differences between the actual structure and the average structure of mixed salts as ascertained by diffraction.

In this case the analysis could proceed to neighbors beyond the second since the the samples are known to be homogeneous and the distribution of the components is random. The analysis of the multiple scatterings between the three atoms comprising the center atom, a nearest neighbor and that fourth neighbor that would be collinear with the first two in the corresponding pure components, found that the three atoms are no longer collinear in the mixture. The XAFS determined the rms angular deviation from collinearity of 7.3±3.0° and 8.2±1.5° for the Rb-Cl-Rb and Rb-Br-Rb atoms, respectively, in $RbBr_{0.62}Cl_{0.38}$. Similarly, the XAFS determined the rms angular deviation from collinearity of 7.7±2.7° and 9.0±1.6° for the Br-K-Br and Br-Rb-Br atoms, respectively, in $Rb_{0.76}K_{0.24}Br$. This buckling is consistent with both the XAFS-determined deviations of the nearest neighbor distances from the average structure ones and the nearest neighbor force constants between the various pairs of atoms, as shown by the molecular-dynamics simulation. The simulation graphically illustrates the local structure and how it deviates from the average in Fig. 9. In fact, this represents a determination of the actual structure as opposed to the periodic average structure determined from diffraction.

It should be emphasized that the determination of the buckling is a direct measurement by XAFS of three-body correlations, and it is only possible with the high accuracy shown here because of very strong multiple scatterings and their high sensitivity to the small deviations from collinearity in this special case of the NaCl-type average structure. Ordinary elastic x-ray or neutron scattering cannot directly determine three-body correlations, but are limited to only two-body correlations. The XAFS results also found that the distance between pairs of atoms and their mean square disorder σ^2 are different between the different component atoms, even at the same neighboring shell, a result which cannot be determined from standard diffraction. The XAFS measurements, together with the information from diffraction that the average structure is a NaCl type, give all the information necessary for a modeling, and, thus, for solving the local structure of the mixed salts by a molecular-dynamic simulation, as shown in Fig. 9.

The buckling could be inferred from the fact that twice the average 1NN distance (denoted in Tables III and IV by brackets enclosing the chemical formula) found by averaging over concentration the respective 1NN bond lengths determined by XAFS for each pair is larger by

0.03 ± 0.022 Å than the 4NN distance. However, this is not convincingly outside the uncertainties. On the other hand the directly measured buckling angle is clearly significant and convincingly proves the presence of buckling. Actually, it is sufficient that the 1NN distance of each component be different from the VCA value for buckling to occur, even if their average is still close to the VCA value. To prove this we have used the values of the 1NN distances presented by Boyce and Mikkelsen[3] for the congruent melting composition of the $Rb_xK_{1-x}Br$ mixed salt [Rb-Br = 3.389 Å, K-Br = 3.319 Å, whose compositional average is the VCA value (Fig. 10)] keeping all other distances the same in a molecular-dynamics simulation. We have found an rms Θ about 0.6° *larger* than the value found for our 1NN distances, but the same within experimental uncertainties. The change in rms Θ is small in this case because the majority atom bond Rb-Br did not change in the simulation, only the smaller concentration one, K-Br. When we changed the Rb-Br distance in our simulation, the rms Θ did change strongly. This test characterizes the different sensitivity of the rms buckling angle to the influence of different atoms in mixture, as well as double-checks our XAFS results.

Although almost no differences (within uncertainties) were observed between the buckling angles of the both systems of mixed salts, the mixture $RbBr_{0.62}Cl_{0.38}$ can be characterized as stronger distorted than the second one, $Rb_{0.76}K_{0.24}Br$. Tables III–VI clearly show that greater deviations from the average structure occurred for the 1NN distributions in the $RbBr_{0.62}Cl_{0.38}$ mixture, in spite of the fact that the initial difference in the size of the two mixing atoms was the same for both systems. Interestingly, as one might expect, the deviations from the average structure in the $A_xB_{1-x}C$ mixture are correlated with the difference in the force constants of the two 1NN pairs: *A-C* and *B-C*. The smaller the difference k_{AC}-k_{BC}, the smaller are the deviations of the atoms from their average sites. In our systems of mixed salts the difference between force constants of Rb-Br and Rb-Cl pairs is larger than that of Rb-Br and K-Br (Table IX). Correspondingly, the mixture $RbBr_{0.62}Cl_{0.38}$ is found to be more distorted than the $Rb_{0.76}K_{0.24}Br$. This is understandable as the positively charged cations are small, tightly bound, while the negatively charged anions are comparatively large, loosely bound configurations of atoms. It takes more energy to distort the cations and thus to mold their size to the average, and it is expected that a disordered sublattice of cations will have more deviation from an average structure.

Our results clearly show that the concept of fixed size bonds in alkali halides as they are mixed is quite incorrect. Substantial changes occurred for the Rb-Cl (0.07 Å) and K-Br (0.09 Å) 1NN distances as their salts were mixed into a single phase. The other point to note from Tables III, IV, VII, and VIII is the comparison of these changes occurring in bond lengths with differences of their σ^2, mean squared disorder, between the mixed salts and the corresponding values of the pure salts. For instance, the Br-K 1NN distance changes from 3.27 Å in the pure salt to 3.36 Å in the mixed salt (Table III) with no significant increase in σ^2 (Table VII). This large change of 0.09 Å with no change in σ^2 indicates that the ions remain in contact and thus their size is concentration dependent. Just the fact that the bond distance changes is, by itself, insufficient evidence of a change in size of the ions because, as pointed out by Ashcroft and Mermin,[26] the ions may be not "touching." The evidence of touching, though, is reflected by the σ^2 since this is a measure, at the low temperatures of the measurements, of the zero point motion and thus the contact force between atoms. The lack of change in σ^2 indicates the same contact force and thus "touching" for both distances of this mixture. In contrast, the Rb-Cl 1NN distance increases in the mixed salt over the pure salt by 0.07 Å (Table IV). Yet the corresponding value of the pure salt σ^2 also almost doubles in the mixture (Table VIII). It suggests that the contact present in the pure salt is loosened in the mixture (and therefore the atoms are no longer "touching") and the increase in bond length should not be interpreted as an increase in ionic size. To verify this conclusion we have studied the Debye-Waller factors of these bonds at 125 K. The results (Tables VII and VIII) show that the Rb-Cl σ^2 in the mixed salt has also a larger temperature dependence than the other 1NN bonds, which is consistent with the conclusion that the atoms are no longer "touching."

First neighbor distances have been measured previously in the same mixed salt systems[3,6] and Fig. 10 presents the result of comparison of Refs. 3, 6 with our data. We have a rather good agreement with published

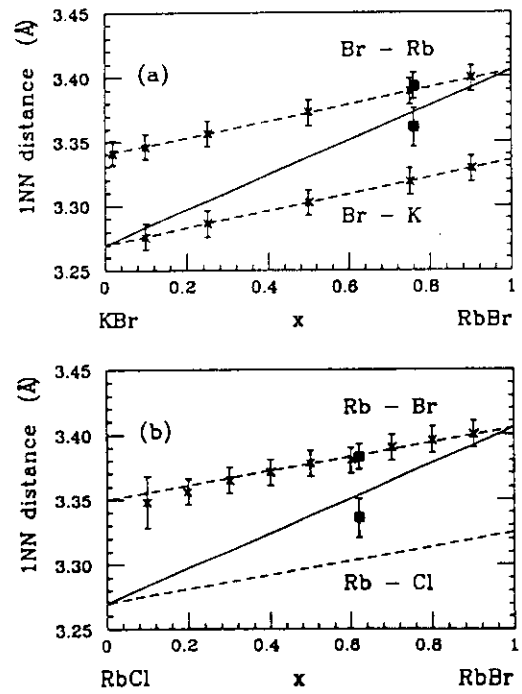

FIG. 10. First nearest neighbor distances (shown by crosses) vs mixture concentration x as determined by (a) Boyce and Mikkelsen (Ref. 3) for Br edge data of $Rb_xK_{1-x}Br$ at 77 K and (b) Sato *et al.* (Ref. 6) for Rb edge data of $RbBr_xCl_{1-x}$ at 77 K. Solid lines follow the VCA. Our experimental points at 30 K are shown by squares on both plots.

data for the longer Rb-Br bond (which contracts under mixing) in both mixtures. However, for the shorter bond, K-Br, which expands under mixing, our result has a larger value than that of Boyce and Mikkelsen.[3] Although this difference appears in Fig. 10(a) to be outside of the uncertainties of Ref. 3, a private communication with Boyce leads us to accept that the real uncertainties in his results may be large enough to cover the disagreement. The solid line in Fig. 10 is the VCA value and in order for the average of the first neighbor distances to agree with the VCA model the shorter bond needs to lie on the lower dashed lines. The results of Boyce and Mikkelsen as displayed in Fig. 10(a) led the authors to argue that the average of the first bond neighbors does satisfy the VCA model; thus a result that they implied was to be expected. However, when one realizes that the buckling does occur, then there is no reason to expect the average of the two 1NN distances to be the VCA value, in agreement with what we find. Our results indicate that it is easier for a shorter bond to expand than for a longer one to contract. This fits the known fact of wider solubility limits of smaller atoms in the midst of larger ones (if other factors are similar) in mixed crystals,[9] and also is as expected from the asymmetric form of the pair potential between atoms where the repulsive force is much larger than the attractive one. Another factor is that one expects that the negatively charged Br ion can be distorted more easily that the positively charged K core and thus it is likely that the negative ion has the more variable size.

In an interesting set of papers,[27] Thorpe and collaborators have calculated the distribution of the disorder about the average zinc-blende or diamond structure for random semiconductor alloys, but did not use this information to try to solve the structure. They assumed that the alloys retain the same elastic constants as the pure constituents and obtain excellent agreement with experimental XAFS measurements of interatomic distances as a function of concentration in most cases. Our results, as discussed just above, show that this assumption of unmodified elastic constants is not valid for the mixed salts, which would lead to an incorrect conclusion about the behavior of the Rb-Cl bond in the mixture.

It should be emphasized that the changes revealed between the pure salts and their mixtures are reliably detected because the theory has been calibrated against the pure salts where the average and local structures are the same. In essence, we are depending on the accuracy of the theory to determine only the changes between the pure and mixed salts and a 10% error in the theory gives only a 10% error in the difference. Thus, the difference is known with greater accuracy than has been estimated in this paper where it was assumed that the errors in the total distance between atoms are uncorrelated between the pure and mixed salts. Only in the determination of Θ_{rms}, the rms buckling angle of the mixture, where the change is directly determined, are the errors not overestimated. It should also be pointed out that the accuracy of our method to determine Θ_{rms} has been proven by testing against $NaTaO_3$ whose value of Θ_{rms} is known at low temperatures from diffraction measurements.[10,15]

The value of Θ_{rms} determined by our measurements is a quadrature sum of contributions from both the buckling and zero point motion. We estimate zero point contribution from the σ^2 listed in Tables VII and VIII. The Θ^v_{rms} due to zero point motion is $2\sigma_1/R_1$ where σ_1 is an average 1NN value of zero point disorder and R_1 is an average 1NN distance, giving $\Theta^v_{rms} = 2.6°$. The factor of 2 comes from the definition of Θ_{rms} which is twice the rms angle between the collinear direction and the 1NN bond. This vibrational contribution causes an increase in Θ_{rms} of less than 7–8 %, and thus is negligible since it is less than the uncertainties.

VIII. SUMMARY AND CONCLUSIONS

The XAFS measurements and data analysis were made of the mixed salts $Rb_xK_{1-x}Br$ and $RbBr_xCl_{1-x}$ at 30 K and 125 K. The concentration x of each mixture was chosen at the minimum congruent melting point. The XAFS results verified that the samples were homogeneous and randomly mixed. Thus it became possible to give a full detailed description of the difference between the actual structure of the mixtures and the average structure as measured by diffraction. The cations in the first mixture and anions in the second one were shown to be shifted from their average sites forming a buckled NaCl-type crystalline structure with an rms angular deviations from collinearity (defined as twice the angle between a 1NN bond and the collinear direction) of 7°–9°. The distance between the nearest atoms deviated from the average values while the σ^2 disorder in these distances depended on the particular pair. A molecular-dynamics simulation using as input parameters the values determined from the XAFS measurements was able to reproduce the measured results and to give a detailed description of the actual structure of the mixture as shown in Fig. 9. Although diffraction determines that the average structure of these mixed salts is a NaCl one, the results presented above solve the actual structure and display the fluctuations about the average.

The deviations from the average are not simply dependent on the difference in sizes of the atoms that are being mixed. In fact, our results, in agreement with others, indicate that the size of an atom is not an accurate concept since it is not fixed. The Rb-Cl and K-Br 1NN distances change by 0.066 ± 0.015 Å and 0.091 ± 0.015 Å, respectively, between the corresponding pure and chosen mixed salts. In addition, the Rb-Cl bond in the mixture becomes much weakened suggesting that the atoms no longer touch, making it no longer meaningful to associate the bond to a size of these atoms which change with concentration. We find it more meaningful to consider both bond lengths and force constants. For example, the mixture $RbBr_xCl_{1-x}$ with a higher difference in 1NN force constants exhibits larger distortions than the other one, $Rb_xK_{1-x}Br$.

The ability of XAFS to determine three-body correlations with high accuracy in the special case of near collinearity deserves a special mention. This feature had been appreciated for some time[28] but the realization of

this potential had to await the development of an accurate theory such as that used in the computer code FEFF5.[13]

The results of this investigation show important differences between the average structure and the real structure of these mixtures. It is clear that any accurate theory of the properties of these mixtures must include these deviations. For example, it has been pointed out that the melting of disordered mixtures depends on deviations from the average structure. The more is the disorder, the greater is the depression of the melting temperature.[8,12] The range of solubility of two components typically depends on the differences in their atomic "sizes;" the greater their difference, the smaller the range. The electrical resistivity, dielectric, optical, and mechanical properties are expected to depend on this disorder as well. Accurate theoretical calculations of the properties of mixed salts and other disordered solids need to account for the deviations of the structure from the average. Our results now permit such calculations to be done since they determine the actual structure. Coordinates of the atomic positions of these salts obtained from MD simulations are available for such purposes.[29]

ACKNOWLEDGMENTS

This work was supported in part by DOE Grant No. DE-FG06-90ER45425 and by the U.S.-Israel BNSF Grant No. 90-00152/1. Two of us (A.F. and A.V.) acknowledge the hospitality of the XAFS laboratory at the University of Washington where the main part of this work was carried out and we all wish to thank B. Ravel, S. Zabinsky, and Professor J. J. Rehr for stimulating discussions.

[1] *Numerical Data and Functional Relationships in Science and Technology*, edited by K.-H. Hellwege and A. M. Hellwege, Landolt-Börnstein, New Series, Group III, Vol. III, Pt. 7a (Springer-Verlag, Berlin, 1973).
[2] A. Frenkel, E. A. Stern, A. Voronel, M. Qian, and M. Newville, Phys. Rev. Lett. **71**, 3485 (1993).
[3] J. Boyce and J. C. Mikkelsen, Jr., Phys. Rev. B **31**, 6903 (1985); J. Boyce (private communication).
[4] A. Yoshiasa, F. Kanamaru, S. Emura, and K. Koto, Solid State Ion. **27**, 267 (1988).
[5] T. Yokoyama, F. Takamatsu, K. Seki, K. Miyake, T. Tani, and T. Ohta, Jpn. J. Appl. Phys. **29**, L1486 (1990).
[6] H. Sato, T. Yokoyama, I. Ono, K. Kaneyuki, and T. Ohta, Jpn. J. Appl. Phys. **31**, 1118 (1992).
[7] Y. T. Tan and K. J. Lushington, J. Phys. Chem. Solids **54**, 309 (1993).
[8] D. Berrebi, L. Grigoryan, S. Rabinovich, E. Shasha, and A. Voronel, J. Phys. Condens. Matter **4**, 10139 (1992).
[9] J. Sangster and A. D. Pelton, J. Phys. Chem. Ref. Data **16**, 509 (1987).
[10] Y. Yacoby and E. A. Stern, Ferroelectrics **125**, 263 (1992).
[11] N. Barkay, A. Levite, F. Moser, and A. Katzir, J. Appl. Phys. **64**, 5256 (1988).
[12] A. Voronel, S. Rabinovich, A. Kisliuk, V. Steinberg, and T. Sverbilova, Phys. Rev. Lett. **60**, 2402 (1988).
[13] J. J. Rehr, R. C. Albers, and S. I. Zabinsky, Phys. Rev. Lett. **69**, 3397 (1992); J. Mustre de Leon, J. J. Rehr, S. I. Zabinsky, and R. C. Albers, Phys. Rev. B **44**, 4146 (1991).
[14] A. I. Frenkel, E. A. Stern, M. Qian, and M. Newville, Phys. Rev. B **48**, 12 449 (1993).
[15] B. Rechav, N. Sicron, Y. Yacoby, B. Ravel, M. Newville, and E. A. Stern, Physica C **209**, 55 (1993).
[16] K.-Q. Lu and E. A. Stern, Nucl. Instrum. Methods Phys. Res. **212**, 475 (1983); E. A. Stern and K. Kim, Phys. Rev. B **23**, 3781 (1981).
[17] M. Newville, P. Livins, Y. Yacoby, J. J. Rehr, and E. A. Stern, Phys. Rev. B **47**, 14 126 (1993).
[18] E. A. Stern, Phys. Rev. B **48**, 9825 (1993).
[19] E. A. Stern and S. M. Heald, in *Handbook on Synchrotron Radiation*, edited by E. E. Koch (North-Holland, New York, 1983), Vol. 1.
[20] E. D. Crozier, J. J. Rehr, and R. Ingalls, in *X-Ray Absorption: Principles, Applications, Techniques of EXAFS, SEXAFS and XANES*, edited by D. C. Koningsberger and R. Prins (John Wiley & Sons, New York, 1988), Chap. 9.
[21] P. R. Bevington, *Data Reduction and Error Analysis for the Physical Sciences* (McGraw-Hill, New York, 1969); W. H. Press, S. A. Teulosky, W. T. Vetterling, and B. P. Flannery, *Numerical Recipes* (Cambridge University Press, New York, 1992).
[22] P. A. Lee and J. B. Pendry, Phys. Rev. B **11**, 2795 (1975).
[23] A. Frenkel, E. Shasha, O. Gorodetsky, and A. Voronel, Phys. Rev. B **48**, 1283 (1993).
[24] A. Nordsieck, Math. Comput. **16**, 22 (1962).
[25] A. I. Frenkel and J. J. Rehr, Phys. Rev. B **48**, 585 (1993).
[26] N. W. Ashcroft and N. D. Mermin, *Solid State Physics* (Saunders, Philadelphia, 1976), pp. 382–385.
[27] Y. Cai and M. F. Thorpe, Phys. Rev. B **46**, 15 872 (1992); **46**, 15 879 (1992); N. Mousseau and M. F. Thorpe, *ibid.* **46**, 15 887 (1992).
[28] B.-K. Teo, J. Am. Chem. Soc. **103**, 3990 (1981).
[29] See AIP document no. PAPS PRBMD-49-11662-24 for 24 pages of coordinates of the atomic positions in the $Rb_{0.76}K_{0.24}Br$ and $RbBr_{0.62}Cl_{0.38}$ clusters. Order by PAPS number and journal reference from the American Institute of Physics, Physics Auxiliary Publication Service, 500 Sunnyside Boulevard, Woodbury, New York 11797-2999. The price is $1.50 for each microfiche (60 pages) or $5.00 for photocopies of up to 30 pages, and $0.15 for each additional page over 30 pages. Airmail additional. Make checks payable to the American Institute of Physics.

Universality of Physical Properties of Disordered Alloys

A. Voronel, S. Rabinovich, and A. Kisliuk
Raymond and Beverly Sackler Faculty of Exact Sciences, School of Physics and Astronomy, Tel Aviv University, 69978 Ramat Aviv, Israel

and

V. Steinberg and T. Sverbilova
Department of Nuclear Physics, Weizmann Institute of Science, 76100 Rehovot, Israel
(Received 27 March 1987; revised manuscript received 5 October 1987)

A simple idea of statistical independence of thermal and chemical disorders in perfectly disordered solid solutions suggests the universality of their thermodynamic and transport properties at high temperatures. Our experimental data on diagrams of state, heat capacities, and resistivities of mixtures of heavy alkali metals convincingly support this idea. A generalization of Lindemann's criterion of melting for disordered alloys has been suggested and applied to a variety of mixtures.

PACS numbers: 64.60.Fr, 64.70.Dv, 65.40.−f, 72.15.Eb

Diagrams of state of binary mixtures of heavy alkali metals K, Rb, and Cs exhibit deep minima with congruent melting at their deepest (azeotropic) points[1] (Fig. 1). These points for $Rb_{0.5}Cs_{0.5}$, $K_{0.5}Cs_{0.5}$, and $Rb_{0.667}K_{0.333}$ offer the rare opportunity to crystallize these alloys from their liquid state without any trace of separation. We have used them to produce samples of perfectly disordered mixed crystals.

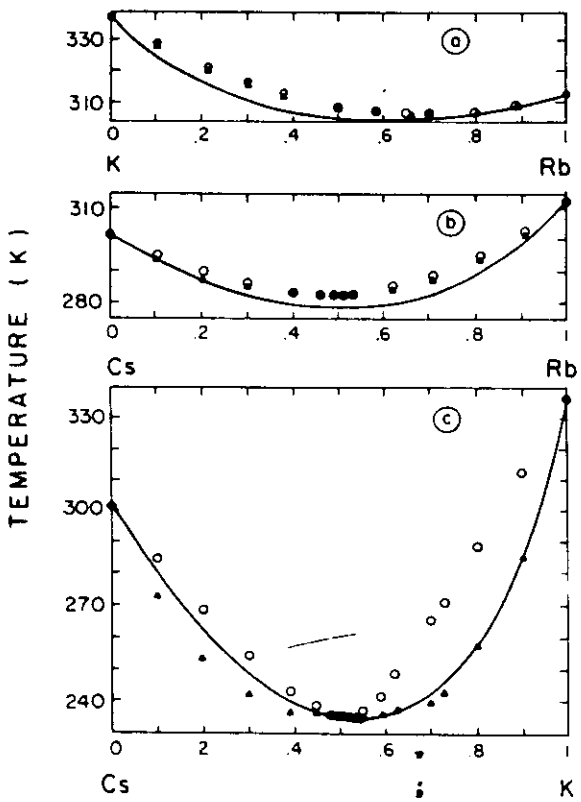

FIG. 1. Diagrams of state of alkali-metal mixtures. The two kinds of points are experimental data (Ref. 1) on freezing and melting temperatures of alloys at corresponding concentrations. The lines are our calculation in accordance with Eq. (4).

The heat capacity of c_p of $K_{0.5}Cs_{0.5}$ and electrical resistivities of $K_{0.5}Cs_{0.5}$, $Rb_{0.5}Cs_{0.5}$, and $Rb_{0.667}K_{0.333}$ have been measured together with their melting temperatures T_m. The experimental technique and sample preparation already have been reported elsewhere.[2,3] The structures, molar volumes, and elasticities of the alloys are similar to or close to additive in the corresponding properties of the pure metals.[4,5] However, their melting temperatures, heat capacities, and electrical resistivities are drastically different (see Figs. 1, 3, and 4).

The amazing result of this study is that these differences can be explained by one simple idea of *statistical independence of thermally induced vibrational disorder of an "averaged" lattice from temperature-independent disorder due to size difference of the constituent atoms.* Our explanation is valid at high temperature ($T > \Theta$, where Θ is the Debye temperature). We

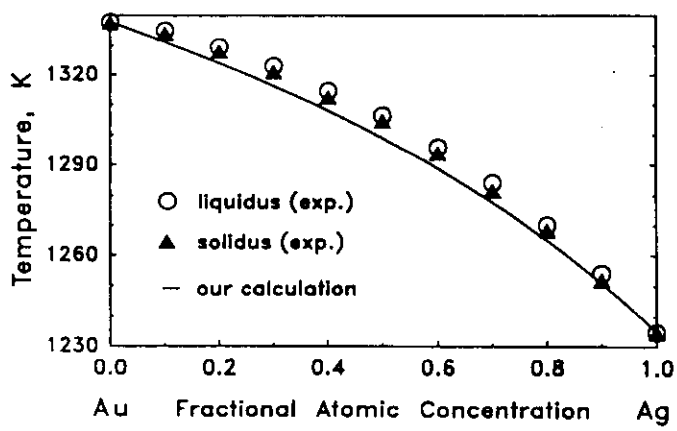

FIG. 2. Diagram of state of Au-Ag alloy. The solid line represents our calculation; the two kinds of points are experimental data on the freezing and melting.

20

have used this idea not only for interpretation of our own data but also to describe some experimental results already known from the literature.[6] It gives a satisfactory quantitative description of phase diagrams for different disordered alloys (see, for example, Fig. 2). The physical properties of these alloys also exhibit a trend to universality, although just on the qualitative level, mostly as a result of imperfection of the samples.

Let us consider the binary solid solution with atoms of two different sizes randomly distributed over a common lattice of the same symmetry as that of the pure components. It is known[7] that an x-ray pattern of such a crystal can be interpreted as a result of superposition of two different patterns corresponding to two different types of disorder.

A mixed lattice which includes atoms of different nature at high temperature produces the same diffraction pattern as would be produced by a simple lattice homogeneously occupied by "averaged" atoms.[7] Thermal motion will cause a reduction of the Bragg-peak intensity which is proportional to the Debye-Waller factor $D=e^{-2W}$, where W is dependent upon a relative mean square uncertainty of equilibrium positions of those "averaged" atoms[8]:

$$W \propto x_t^2 = \frac{\langle(\Delta r)_t^2\rangle}{d_{12}^2} = \frac{9\hbar^2 T}{M_{12}k_B\Theta_{12}^2 d_{12}^2}. \quad (1)$$

Here $M_{12}=p_1M_1+p_2M_2$ ("average" mass of atom of the mixture with concentrations p_1,p_2), $\Theta_{12}^{-2}=p_1\Theta_1^{-2}+p_2\Theta_2^{-2}$ ("average" Debye temperature[9]), and $d_{12}=p_1d_1+p_2d_2$ (average nearest-neighbor distance[4]). Meanwhile, a size disorder emerging from a mismatch of atoms will manifest itself like a "frozen heat motion" and introduces an additional reduction[7] $D'=e^{-2W'}$ dependent upon a relative mean square uncertainty of the atomic size: $x_{12}^2=4\langle(\Delta r_{12})^2\rangle/d_{12}^2$. The intensity which is lost by the diffraction peaks because of size dispersion of the scatterers appears in a diffuse background caused just in the same way as happens because of uncertainty of the scatterers' position from thermal motion. Indeed, such a strong, temperature-independent, diffuse background has been observed on the x-ray pattern of our $K_{0.5}Cs_{0.5}$ mixed crystal.[10] The simplest assumption is that these two scattering factors are uncorrelated. Therefore, for a perfectly disordered mixed crystal the total reduction of the integrated intensities of the Bragg peaks can be presented as a generalized Debye-Waller factor $D_g=DD'$. This assumption was used first for interpretation of x-ray patterns of disordered solid solutions by Guinier.[7]

Let us introduce now a corresponding definition of a generalized mean square uncertainty of the atomic coordinate in the mixed crystal, which Guinier has never used:

$$x^2 \equiv \frac{\langle(\Delta r)^2\rangle}{d_{12}^2} = \frac{\langle(\Delta r)_t^2\rangle}{d_{12}^2} + \frac{4\langle(\Delta r_{12})^2\rangle}{d_{12}^2}. \quad (2)$$

Generally speaking, a symmetry-dependent numerical coefficient can multiply the second term. This definition means that one can postulate a new generalized Lindemann criterion of melting for disordered alloys analogous to that of the pure substances[8] as a natural limitation of the relative atomic-coordinate uncertainty within the crystalline state. It is clear that such a criterion will set up a limit not only for the vibration amplitude but for the size dispersion in a real mixed crystal as well.[11]

Combining (1) and (2), one has to assume, as has been done for the pure crystals,[8] that the total relative mean square uncertainty should be always below a certain value x_m^2:

$$\frac{9\hbar^2 T}{M_{12}k_B\Theta_{12}^2 d_{12}^2} + \frac{4\langle(\Delta r_{12})^2\rangle}{d_{12}^2} \le x_m^2, \quad (3)$$

which gives the following equation for the melting temperature:

$$T_m = \frac{M_{12}k_B\theta_{12}^2 d_{12}^2}{9\hbar^2} x_m^2 \left(1 - \frac{4\langle(\Delta r_{12})^2\rangle}{x_m^2 d_{12}^2}\right). \quad (4)$$

The next crucial step in our approach is the calculation of a second term in Eqs. (2) and (4) based on a concept of a temperature-dependent hard-sphere diameter of an atom.[12]

The recent development of density-functional theory confirms both the validity of the Lindemann criterion for freezing of a hard-sphere liquid[13] and the applicability of the hard-sphere model to freezing of binary mixtures.[14] Therefore we define the average uncertainty of atomic radius as $\langle(\Delta r_{12})^2\rangle=p_1p_2(r_1-r_2)^2$, where r_1 and r_2 are temperature-dependent hard-sphere radii taken from Ref. 12.

One can see from Fig. 1 that the melting temperatures calculated from Eq. (4) agree with the experimental

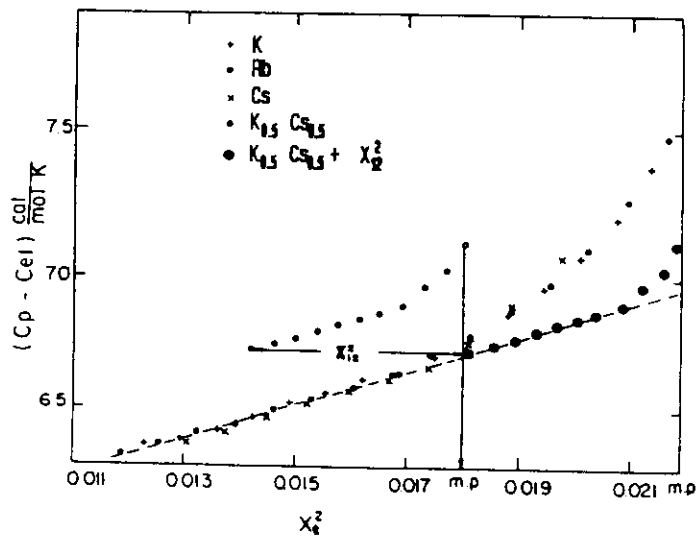

FIG. 3. Heat capacities $c=c_p-c_{el}$ of K, Rb, Cs, and $K_{0.5}Cs_{0.5}$ vs mean square uncertainty x_t^2.

21

values[1] which we have also checked in our own measurements. This calculation fits the experimental data much better than the corresponding calculation based on pseudopotential theory.[5] In Fig. 2 one also can see that Eq. (4) works well for Ag-Au solid solution. Here the size dispersion is small and the melting almost exactly corresponds to a prefactor in the Eq. (4).

In Fig. 3 the data on the lattice heat capacities $c = c_p - c_{el}$ (c_{el}, the electron heat capacity, was subtracted from the measured c_p following MacDonald, Shukla, and Kahaner[15]) of pure K, Rb, and Cs are plotted together with $K_{0.5}Cs_{0.5}$ as functions of the parameter x_t^2 characterizing only the thermally induced disorder. At high temperature [see Eq. (1)] this parameter is almost proportional to T.[8] One can see that c of a pure metal is close to a linear universal function of x_t^2 till it reaches about $0.8T_m$. Then the function ceases to be linear (because of vacancy formation and/or strong deviation from harmonicity) but does not cease to be universal.[16] The data on $K_{0.5}Cs_{0.5}$ appear to be strongly separated from this line. However, if instead of x_t^2 one uses the generalized parameter x^2 defined by Eq. (2), our experimental points for $K_{0.5}Cs_{0.5}$ fall on a continuation of the universal curve for pure metals with an accuracy better than 1%. The melting point of the alloy also excellently corresponds to the same value of the Lindemann constant $x^2 = x_m^2$ (see Fig. 1).

The interpretation of our resistivity data (Fig. 4) is even more striking. The mean free path of an electron is defined in the deformation-potential approximation[8] by a local relative fluctuation of volume Δ ($\Delta \equiv \Delta V/V$): $\lambda^{-1} \simeq N\bar{\sigma}\langle\Delta^2\rangle$ (N is a number density and $\bar{\sigma}$ a total cross section). We can again use Eq. (2) rewritten to correspond to relative fluctuation of volume under the same assumption of statistical independence of thermal fluctuations of scatterers from their size dispersion. It leads to the well-known Matthiessen's rule[17]:

$$\rho = \frac{\hbar}{e^2}\frac{k_F}{n}\left(\frac{1}{\lambda_t} + \frac{1}{\lambda_{12}}\right). \tag{5}$$

Here k_F is the Fermi wave number and n is the electron concentration. The electron's mean free path due to thermal lattice vibrations λ_t has already been calculated[8]: $\lambda_t^{-1} \simeq n\bar{\sigma}\frac{2}{3}x_{tm}^2 T/T_m$, where x_m^2 is the value of x_t^2 at the melting point of the alloy.

Simple calculation of a term defined by the size difference in Eq. (5) gives for the bcc structure

$$\lambda_{12}^{-1} = n\bar{\sigma}\tfrac{9}{32}p_1p_2(V_1 - V_2)^2/(p_1V_1 + p_2V_2)^2. \tag{6}$$

Atomic volumes V_1 and V_2 should be calculated in this case from radii corresponding to electron scattering.[18] One can notice that Eq. (6) gives a generalization of the well-known Nordheim rule (and Mott's rule as its consequence), namely, that the residual resistivity of an alloy constituted from elements with close atomic volumes is proportional to p_1p_2.[19]

To single out the size-dependent effect, we have plotted reduced resistivities ρ/ρ_m (ρ_m is the resistivity of a crystal at T_m) versus reduced temperature T/T_m:

$$\frac{\rho}{\rho_m} = \frac{\frac{2}{3}x_{tm}^2 T/T_m + \frac{9}{32}p_1p_2(r_1^3 - r_2^3)^2/(p_1r_1^3 + p_2r_2^3)^2}{\frac{2}{3}x_{tm}^2 + \frac{9}{32}p_1p_2(r_1^3 - r_2^3)^2/(p_1r_1^3 + p_2r_2^3)^2}. \tag{7}$$

In Fig. 4 one can see the agreement of our experimental data with the universal Eq. (7). The deviation of the measured points from Eq. (7) at higher temperature for all alloys, but especially for $Rb_{0.667}K_{0.333}$, is easily explained by a premelting phenomenon. This phenomenon affects the two other alloys in a much milder way because of their lower melting points. From Fig. 3 one can see that the premelting phenomenon for the low-melting alloy $K_{0.5}Cs_{0.5}$ is much smaller than for pure elements (and for the high-melting alloy K-Rb correspondingly).

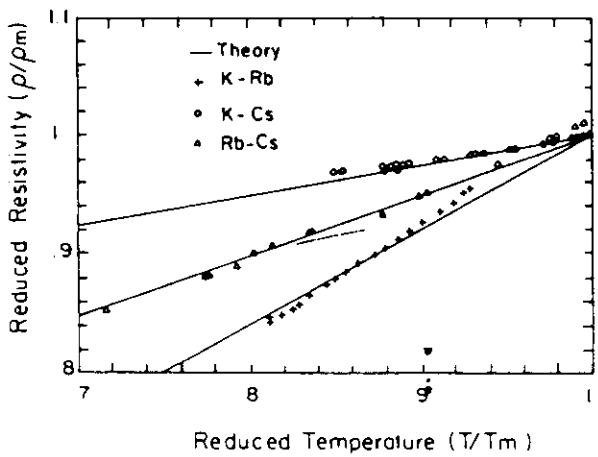

FIG. 4. Reduced resistivities of alkali-metal alloys below their melting points.

Thus, we have demonstrated that the idea of statistical independence of thermal fluctuations and size dispersion, when applied to alkali-metal disordered alloys, leads to impressive quantitative universality in macroscopic properties. The key point of our experimental study is the possibility of preparing fully disordered mixed crystals at the azeotropic points of diagrams without a trace of partial ordering or inclusions of other phases. In principle, such a high degree of disorder is achievable for any concentration of a disordered alloy. However, practically, it requires extremely long annealing times, maybe as long as several months.[20] Nevertheless, when the same idea is used to describe various binary (Au-Ag, Ar-Kr, and other) as well as ternary (K-Rb-Cs) alloys, the diagrams of state show remarkable agreement with experimental

22

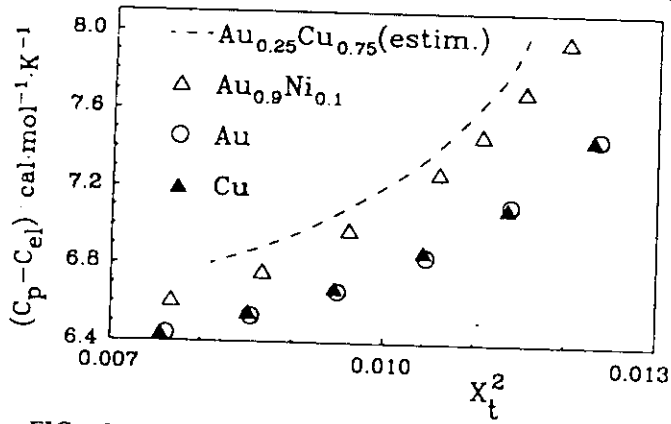

FIG. 5. Heat capacities $c=c_p-c_{el}$ of Cu, Au, and $Au_{0.9}Ni_{0.1}$, $Au_{0.25}Cu_{0.75}$ vs mean square uncertainty x_t^2. The experimental data on Cu, Au, and $Au_{0.9}Ni_{0.1}$ are taken from Ref. 6. The dashed curve is assumed in accordance with our evaluation of the poor data of both Refs. 6 and 22.

data taken from literature.[21] Unfortunately, the experimental data on heat capacity and resistivity are much more sensitive to the quality of samples, and they scatter too much to be conclusive. Nevertheless, in spite of the low accuracy of published data at high temperatures, the positive deviations from additivity (Kopp's rule) of c_p analogous to Fig. 3 has been reported for many disordered systems[6] (Au-Cu, Cu-Mg, Au-Zn, Au-Ni, Cu-Ni, Cu-Zn, Pb-In, and In-Tl). Moreover, our analysis of disordered alloys with the same fcc structure ($Au_{0.25}Cu_{0.75}$ and $Au_{0.9}Ni_{0.1}$—Fig. 5) shows a qualitatively correct trend: The more the size dispersion, the higher the positive deviation from Kopp's rule. The values of x_t^2 for fcc metals differ from those in Fig. 3 in accordance with the difference in symmetry.

We are grateful to M. Azbel, D. Bergman, P. Bak, H. Ch. Andersen, J. P. Hansen, and J. Adler for useful discussions. This work was supported in part by the Israel–U.S. Binational Science Foundation.

[1]*Handbook of Thermal and Transport Properties of Alkali Metals*, edited by R. W. Ohse (Blackwell Science, Oxford, 1985).

[2]A. Voronel, V. Steinberg, and T. Sverbilova, Phys. Lett. **79A**, 180 (1980).

[3]V. Steinberg, T. Sverbilova, and A. Voronel, J. Phys. Chem. Solids **42**, 23 (1981).

[4]B. Bohm and W. Klemm, Z. Anorg. Allg. Chem. **243**, 69 (1939).

[5]T. Soma, H. Matsuo, and M. Funaki, Phys. Status Solidi (b) **108**, 221 (1981).

[6]R. Hultgren *et al.*, *Selected Values of Thermal Properties of Binary Alloys* (American Society for Metals, Metal Park, OH, 1973); M. Hansen and K. Anderko, *Constitution of Binary Alloys* (McGraw-Hill, New York, 1958).

[7]A. Guinier, *X-Ray Diffraction* (W. H. Freeman, San Francisco, 1963).

[8]J. M. Ziman, *Principles of the Theory of Solids* (Cambridge Univ. Press, Cambridge, 1972).

[9]G. Grimvall, *Thermal Properties of Materials* (North-Holland, Amsterdam, 1986).

[10]U. Shmueli, V. Steinberg, T. Sverbilova, and A. Voronel, J. Phys. Chem. Solids **42**, 19 (1981).

[11]The assumption that a lower limit for a mixture's melting temperature coincides with its virtual glass point [see A. Voronel and S. Rabinovich, J. Phys. F **17**, L193 (1987)] leads to an equation for concentration p at a certain ratio of the radii. We get the limit of mutual solubility of hard spheres at $r_1/r_2\simeq 0.84$ in good agreement with the empirical Hume-Rothery rule [see J. H. Barrat, M. Baus, and J. P. Hansen, Phys. Rev. Lett. **56**, 1063 (1986)].

[12]P. Protopapas, H. Ch. Andersen, and N. Parlee, J. Chem. Phys. **59**, 15 (1973).

[13]W. Curtin and N. W. Ashcroft, Phys. Rev. Lett. **56**, 2775 (1986).

[14]Barrat, Baus, and Hansen, Ref. 11.

[15]R. A. MacDonald, R. C. Shukla, and D. K. Kahaner, Phys. Rev. B **29**, 6489 (1984).

[16]Let us assume that monovacancy formation plays a major role in deviation from linearity of the lattice heat-capacity curve near the melting point. Then a corresponding contribution

$$\Delta c_{vac}\propto(\Delta E/k_BT)^2\exp(-\Delta E/k_BT),$$

where ΔE is a formation energy, is a universal function of a dimensionless parameter $\Delta E/k_BT$. Since the total heat capacity remains also a universal function of the parameter x_t^2 (see Fig. 2) one has to expect proportionality between these two parameters: $k_BT/\Delta E\propto x_t^2$. Using Eq. (1) we see that this relation coincides with the known expression for the vacancy formation energy $\Delta E\propto(3\hbar)^{-2}Mk_B\Theta^2\sigma^2$ [K. Mukherjee, Philos. Mag. **12**, 915 (1965)].

[17]I. M. Lifshits, M. Ya. Azbel, and M. I. Kaganov, *Electron Theory of Metals* (Consultants Bureau, New York, 1973).

[18]W. H. Harrison, *Electronic Structure and Properties of Solids* (W. H. Freeman, San Francisco, 1980).

[19]J. M. Ziman, *Electrons and Phonons* (Clarendon, Oxford, 1960).

[20]L. Elford, F. Muller, and O. Kubaschewski, J. Phys. Chem. **26**, 607 (1965).

[21]S. Rabinovich, A. Voronel, and L. Peretzman, to be published.

[22]M. Hirabayashi, S. Nagasaki, and H. Kono, J. Appl. Phys. **28**, 1070 (1957).